ELECTROCHEMICAL DETECTION OF BENZO[*A*]PYRENE-INDUCED DNA DAMAGE AT TP53 OLIGOMERS: IMPACT OF 5' – METHYL CYTOSINE AND BIOACTIVATION ON THE GENOTOXICITY PROCESS.

By

Caitlin M. Trumbo

July, 2014

Director of Thesis/Dissertation: Dr. Eli Hvastkovs

Major Department: Chemistry

DNA houses the blueprint that dictates how an organism will develop. However, DNA features numerous reactive sites that can be attacked by chemicals and radiation, resulting in DNA damage and possibly mutations. Chemical products and other environmental toxins must be tested for genetic abnormalities due to exposure. Traditional DNA damage detection can be tedious, time-consuming, and cost prohibitive. Electrochemical methods to detect DNA damage offer remedies to these drawbacks. Simple and sensitive DNA hybridization sensors are widely used for DNA detection and studying biochemical processes at specific DNA sequences.

An electrochemical DNA hybridization sensor designed to detect DNA damage at hotspot TP53 gene sequences resulting from bioactivated benzo[*a*]pyrene (BP) will be discussed. TP53 codes for the p53 protein, and mutations at the studied genetic sequence have been shown to be prevalent in many different cancers. Double stranded DNA 21-mers were absorbed on gold electrodes followed by adsorption and saturation with a heme enzyme model, myoglobin. Myoglobin was activated using hydrogen peroxide and exposed to solutions of BP, which allowed BP to be oxidized into reactive metabolites. DNA damage was detected voltametrically by charting changes in square wave voltammetric signals due to a redox-active di-viologen

derivative that has been shown to bind to DNA in a structure-specific manner. Aspects of the sensor optimization process will be discussed including how BP stereochemistry and epigenetic factors influence the voltammetry, the impact of myoglobin non-specific adsorption on the electrode surface, and numerous control reactions designed to show that bioactivated reactive metabolites were detected at the DNA sequence. Overall, the incorporation of enzymes with a DNA hybridization interface has opened up new possibilities to utilize more biologically relevant enzymes, such as cytochrome P450s, to study of important metabolic related DNA damage processes at specific gene sequences.

ELECTROCHEMICAL DETECTION OF BENZO[*A*]PYRENE-INDUCED DNA DAMAGE AT TP53 OLIGOMERS: IMPACT OF 5' – METHYL CYTOSINE AND BIOACTIVATION ON THE GENOTOXICITY PROCESS.

A Thesis

Presented To the Faculty of the Department of Chemistry

East Carolina University

In Partial Fulfillment of the Requirements for the Degree

Masters of Science in Chemistry

by

Caitlin M. Trumbo

July, 2014

ELECTROCHEMICAL DETECTION OF BENZO[*A*]PYRENE-INDUCED DNA DAMAGE AT TP53 OLIGOMERS: IMPACT OF 5' – METHYL CYTOSINE AND BIOACTIVATION ON THE GENOTOXICITY PROCESS.

by

Caitlin M. Trumbo

APPROVED BY:

DIRECTOR OF
DISSERTATION/THESIS: _____
Eli G. Hvastkovs, Ph.D.

COMMITTEE MEMBER: _____
Allison S. Danell, Ph.D.

COMMITTEE MEMBER: _____
Yu Yang, Ph.D.

COMMITTEE MEMBER: _____
Anthony Kennedy, Ph.D.

COMMITTEE MEMBER: _____
Ann O. Sperry, Ph.D.

CHAIR OF THE DEPARTMENT
OF CHEMISTRY: _____
Allison S. Danell, Ph.D.

DEAN OF THE
GRADUATE SCHOOL: _____
Paul J. Gemperline, Ph.D.

ACKNOWLEDGEMENTS

I would like to thank my research advisor, Dr. Eli Hvastkovs, as well as my thesis committee Dr. Allison Danell, Dr. Yu Yang, Dr. Anthony Kennedy, and Dr. Ann Sperry for their support, guidance, help, and patience throughout my Master's program.

I would also like to thank my parents for providing with me the opportunity to pursue this degree as well as provide me with the necessary tools to be successful in life.

Last, I would like to thank my friends for their support, encouragement, and patience that enabled me to complete this work. Without them I would not have been able to complete this degree.

TABLE OF CONTENTS

LIST OF TABLES

LIST OF FIGURES

LIST OF SYMBOLS AND ABBREVIATIONS

5-meC	5-methylcytosine
Γ_0	Amount of RuHex bound at the electrode surface (mol/cm^2)
A	Ampere
Ar	Argon
N_A	Avogadro's number
BP/B[*a*]P	Benzo[*a*]pyrene
BPDE	Benzo[*a*]pyrene-7,8-dihydrodiol-9,10-epoxide
BHA	Butylated hydroxyanisole
C12-viologen	$C_{12}H_{25}V^{2+}C_6H_{12}V^{2+}C_{12}H_{25}$ (V^{2+} is 4,4'-bipyridyl or viologen)
°C	Celsius
Cm	Centimeter
Q	Charge (μC, C)
Q_{diff}	Charge from diffusion
Q_{surf}	Charge from surface bound species
Z	Charge of the redox molecule
Q_{dl}	Charge, capacitive/double layer
CC	Chronocoulometry
C	Complementary
con	Control
C	Coulomb
CV	Cyclic voltammetry
cyt P450	Cytochrome P450

CPR	Cytochrome P450 reductase
CpG	Cytosine – phosphate – guanine
DI H_2O	Deionized water
DNA	Deoxyribonucleic acid
K_2HPO_4 (HPO_4^{2-})	Dipotassium phosphate
DTT	Dithiothreitol
Γ_{DNA}	DNA probe surface density (molecules/cm^2)
PNA	DNA-peptide nucleic acid
dsDNA	Double-stranded DNA
E-buffer	Electrochemical buffer
A	Electrode area (cm^2)
e^-	Electrons
EH	Epoxide hydrolase
EDTA	Ethylenediaminetetraacetic acid
F	Faraday's constant
Au	Gold
G	Gravitational acceleration
Hz	Hertz (s^{-1})
H_2O_2	Hydrogen peroxide
LbL	Layer-by-layer
LC-MS	Liquid chromatography – Mass spectrometry
$LiClO_4$	Lithium perchlorate
MCH	Mercaptohexanol

me	Methyl
MB^+	Methylene blue
µA	Microampere
µC	Microcoulomb
µL	Microliter
µm	Micrometer
µM	Micromolar
mg	Milligram
mL	Milliliter
mm	Millimeter
mM	Millimolar
mΩ	Milliohm
mV	Millivolt
min	Minutes
M	Molar
mol	Moles
KH_2PO_4 ($H_2PO_4^-$)	Monopotassium phosphate
Mb	Myoglobin
Nm	Nanometer
nM	Nanomolar
NADPH	Nicotinamide adenine dinucleotide phosphate
N_2	Nitrogen
M	Number of bases in the DNA

N	Number of electrons per molecule for reduction
i_p	Peak current ratio
KCl	Platinum chloride
Pt	Platinum wire
PAH	polycyclic aromatic hydrocarbon
PEG	Polyethylene glycol
PCR	Polymerase chain reaction
E	Potential (V)
P	Probe
RPM	Rates per minute
RuHex	Ruthenium (III) hexamine
S	Seconds
Ag/AgCl	Silver/Silver chloride
ssDNA	Single-stranded DNA
NaCl	Sodium chloride
SWV	Square wave voltammetry
H_2SO_4	Sulfuric acid
THF	Tetrahydrofuran
T	Time
TEA	Triethylamine
Tris base (Tris)	Tris(hydroxymethyl) aminomethane
Tris-HCl	Tris(hydroxymethyl) aminomethane hydrochloride
TE Buffer	Tris-EDTA buffer

UV-Vis	Ultraviolet-Visible
V	Volts
w/v	Weight by volume
wt	Wild type

CHAPTER 1: INTRODUCTION

DNA Damage from Xenobiotics

Living organisms are constantly exposed to substances, known as xenobiotics, which are not produced endogenously in the body. [1-3] Xenobiotics enter the body from a multitude of sources: pharmaceutical ingestion, illicit drug or alcohol abuse, environmental pollution of food and water, and chemicals in the workplace. [3] Due to the potentially dangerous effects as well as the cumulative dosage of these substances, long term exposure to these substances can eventually cause serious health problems. [2]

Bioactivation

Living organisms have the ability to eliminate xenobiotics once exposure has occurred. Hydrophobic xenobiotics must be made more hydrophilic before excretion can take place. The human body imparts hydrophilicty to hydrophobic xenobiotics though a series of metabolic reactions. An example of how this would occur is in the elimination of hydrophobic benzo[*a*]pyrene (BP), a chemical primarily found in cigarette smoke, which is shown in **Figure 1.1**. Human exposure to BP occurs most often by ingestion, inhalation, and dermal absorption. Exposure to BP most often occurs during smoking, but can also occur during the consumption of charbroiled foods. [4] Oxidative enzymatic reactions make the highly hydrophobic planar polyaromatic hydrocarbon (PAH) slightly less so. [5] However, while metabolism works to help to eliminate substances from the body, it can often produce a more reactive substance via the same metabolism processes designed to eliminate the substance from the body. [3] When xenobiotics are converted into reactive and toxic metabolites inside the body via a metabolism process this is

known as bioactivation. [2,3,5] **Figure 1.1** shows BP, likely in a complex compound mixture, metabolized into benzo[*a*]pyrene-7,8-diol-9,10-epoxide (BPDE), by cytochrome (cyt) P450 enzymes in the body. BPDE is a highly reactive diol epoxide that can react with nucleophilic molecules in the body.

Genotoxicity

Bioactivated, reactive metabolites may bind to biomolecules, such as DNA, causing damage, also known as genotoxicity. Genotoxicity can result in genetic modifications, cellular damage, and major health problems, such as cancer. [5] Mutations that alter the function of specific genes such as tumor suppressor genes, which are critical for cell division, allow cancerous tumors to form. [1] Cigarette smoke, which contains many xenobiotics, has been shown to induce tumors in rodents. [6]

BP bioactivation and the subsequent genotoxicity that results is also shown in **Figure 1.1**. Benzo[*a*]pyrene is strongly implicated in the development of lung cancer, which is currently the leading cause of cancer death in the United States. [7] BPDE, a chemically reactive electrophile, can react with nucleophilic sites on DNA, which results in BPDE adducted DNA. If not repaired correctly by separate cellular processes, these DNA adducts can lead to base mutations and eventually cellular carcinogenesis **(Figure 1C, D)**. [7,8]

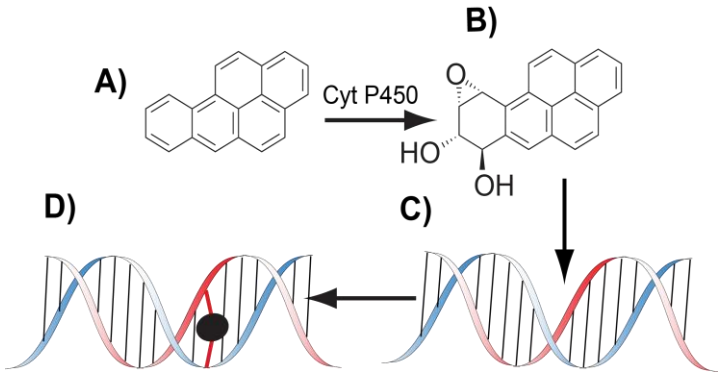

Figure 1.1. Bioactivation of A) BP to B) BPDE by cyt P450 in the body, followed by C) exposure to DNA, and eventual D) DNA damage.

Sequence Specific Genotoxicity

DNA mutations due to xenobiotic exposure occur more often at certain sequences in the genome, termed hotspots.[7,9] For instance, about 60% of human lung cancers contain mutations at specific sites in the TP53 tumor suppressor gene.[7] The TP53 gene codes for the p53 tumor suppressor protein, which plays an important role in cell division and apoptosis.[10-14] Mutations along the TP53 gene are normally found at sites featuring a cytosine-guanine sequence (CpG) at codons 157, 248, and 273, which correspond to amino acids within the DNA binding domain of p53.[7,9] Typically, BP metabolites attack the N2 position of the guanines at these sites as shown in **Figure 1.2**.[7] The figure shows how the unrepaired, adducted guanine damage can result in an alternate base upon replicative cellular processes, which then changes the gene sequence. The figure shows a guanine to thymine transversion, which results in a mutated sequence and mutant p53 transcription products.[7,15,16]

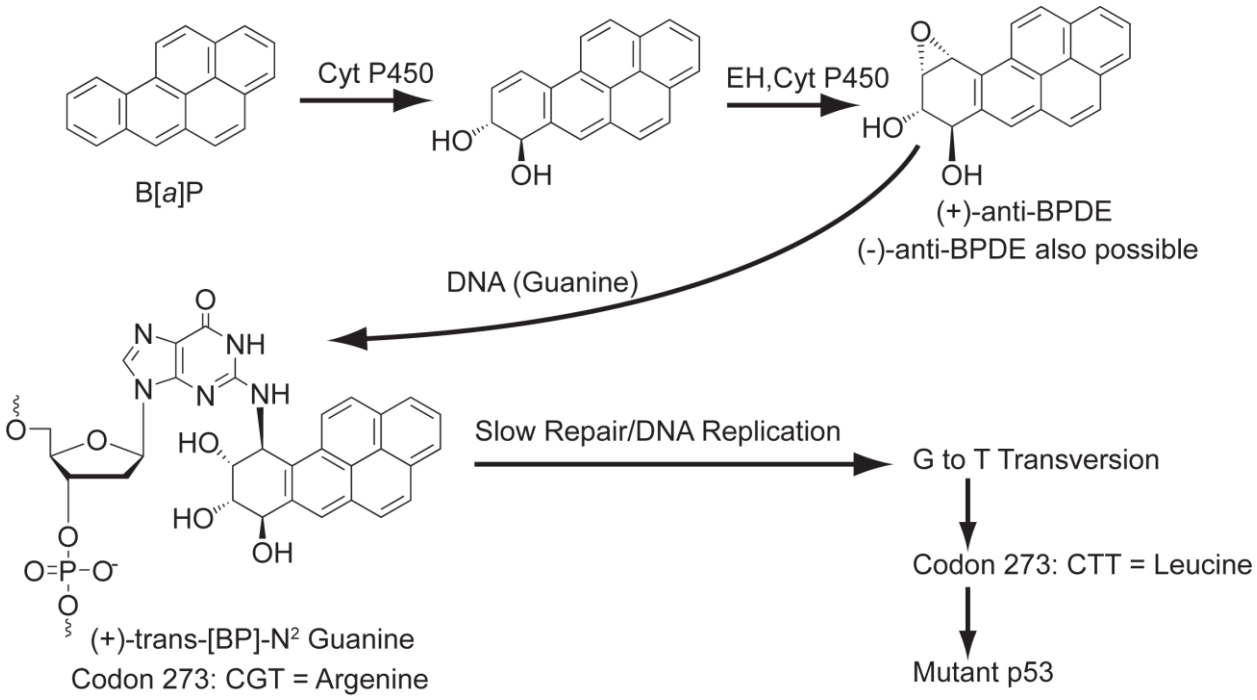

Figure 1.2. Mechanism of benzo[*a*]pyrene induced DNA adduct formation at TP53 hotspot codon 273. Under normal conditions, guanine pairs with cytosine via three hydrogen bonds. However, when BPDE is present, one of the hydrogen bonds at the N2 position of the guanine is used to form a BPDE-DNA adduct. Guanine is then unable to bind cytosine; therefore, it must pair with adenine using its remaining two hydrogen bonds. This causes a guanine to thymine transversion during replication, which in turn causes mutant p53. [3]

BPDE Stereoisomers

Metabolism produces several different BPDE stereoisomers. Four different metabolites are possible, (−)-*syn*-BPDE, (+)-*syn*-BPDE, (−)-*anti*-BPDE, and (+)-*anti*-BPDE, where the (+/−) denotes the orientation of the hydroxyl group at carbon 8 (C8) adjacent to the epoxide at C9 and C10 in the BP molecule. For instance, (+)- denotes that the epoxide and hydroxyl group are angled away from the observer if the molecule was placed flat, like that shown in **Figure 1.3**. The *syn/anti* denotation refers to how the epoxide and the hydroxyl group at C7 are aligned relative to the other. *Anti*- terminology refers to how the epoxide and the hydroxyl at C8 are on

opposite planes of the BP molecule. This is also shown in **Figure 1.3**. In vivo, the *anti*-BPDE metabolites have been shown to be much more mutagenic and carcinogenic; [17] therefore, in the experiments described herein *anti*-BPDE conformations were utilized. Enantiomerically pure (+)-*anti*-BPDE as well as racemic (±)-*anti*-BPDE were used in order to study the effect of different stereochemical BPDE conformations on adduct formation. The racemic BPDE mixture contains both (−)-*anti*-BPDE and (+)-*anti*-BPDE at a 50/50 ratio, while the enantiomerically pure solution contains only (+)-*anti*-BPDE. [18]

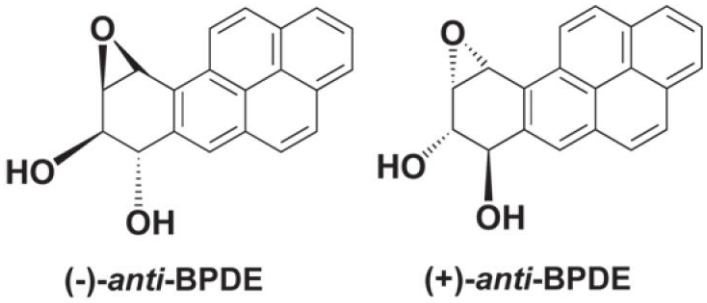

Figure 1.3. *anti*-BPDE stereoisomers.

DNA Damage Influenced by Epigenetic Modifications

Modifications to DNA that do not alter the base sequence are termed epigenetic modifications. [19] One such modification that plays an important role in bioactivation and genotoxicity is cytosine methylation, which occurs when the cytosine 5' to the guanine in the aforementioned CpG sites is methylated at the 5-carbon (5-meC). [19-21] Methylated cytosine is seen in **Figure 1.4**. The patterns of DNA methylation are non-random, well regulated, and tissue-specific. [22] The aforementioned hotspots in the TP53 gene contain 5'-CpG-3' sequences,

and the cytosine is known to be methylated at these sites in all human tissues. [20,23] Cytosine methylation is essential for normal development and is involved in many endogenous processes such as genomic imprinting, X chromosome inactivation and cell differentiation. [20,22]

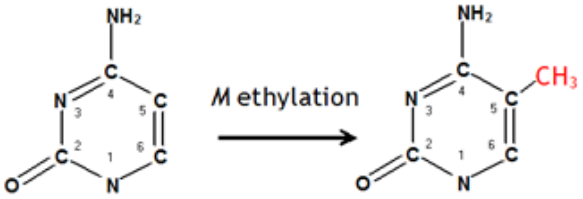

Figure 1.4. Methylation at the 5-carbon of cytosine.

Studies have shown that cytosine methylation at these CpG sites is the primary factor which directs preferential binding of BPDE to the DNA. [20,24] The methyl group in a methylated cytosine protrudes into the major groove, which enhances the hydrophobicity of the molecule and environment at the CpG site, and favors the binding of BPDE at these sites. Also, it has been shown that repair of damage, caused by interactions with bulky chemicals, at these sites is significantly slower than repair at other sites. [20] Due to the influence of cytosine methylation on the formation and structure of BPDE-DNA adducts, this epigenetic modification was studied to provide insight into epigenetic influences and implications associated with such modifications.

Detection of Site-Specific DNA Damage

DNA Hotspot Detection

A method that has been used to identify several DNA damage hotspots resulting from exposure to xenobiotics involves exposing the xenobiotic of interest to a cell model followed by isolation of the genomic DNA. The DNA can be then treated with UvrABC nuclease, a DNA nucleotide excision repair enzyme, which cleaves the DNA adducts at specific nucleobase sites before and after the DNA adduct. A set of specialized PCR protocols is followed to generate a sample of DNA with varying lengths. The PCR products are then separated by gel electrophoresis, and sequenced. [7,16,20,24-29] Despite the wealth of information that this protocol can generate, the method to detect hotspot damage location can be time consuming, labor intensive, and expensive. The impetus for the presented research is to explore a sensor approach that has the ability to alleviate these drawbacks.

DNA Damage Detection

One way to detect DNA damage is through the use of electrochemical biosensors. In contrast to the methods described above, electrochemical DNA biosensors are low cost, simple, and sensitive. In general, an electrochemical DNA biosensor consists of two parts: a biorecognition element (also known as the molecular recognition layer) which allows the selective detection of the analyte, and a signal transducer which converts the recognition event to a measurable signal. [30] Several types of electrochemical DNA sensors have been described with various uses. [31] Higher throughput methods have been developed to detect DNA damage. [32] Such methods include the detection of xenobiotic adducts [33] or the production of reactive

metabolites.[34,35] These methods have employed electrochemiluminescent detection and LC-MS techniques to provide relative rates of DNA damage.[33,34] DNA damage can also be detected using thin films containing alternating layers of DNA and enzymes known as the layer-by-layer (LbL) method.[36] While these methods are effective in generating information about DNA damage, more specific information such as DNA damage site or adduct orientation cannot be determined. Since these are vital components in understanding how genotoxicity results in genomic mutations, new strategies must be explored to detect these DNA damage aspects.

Electrochemical DNA Hybridization Detection

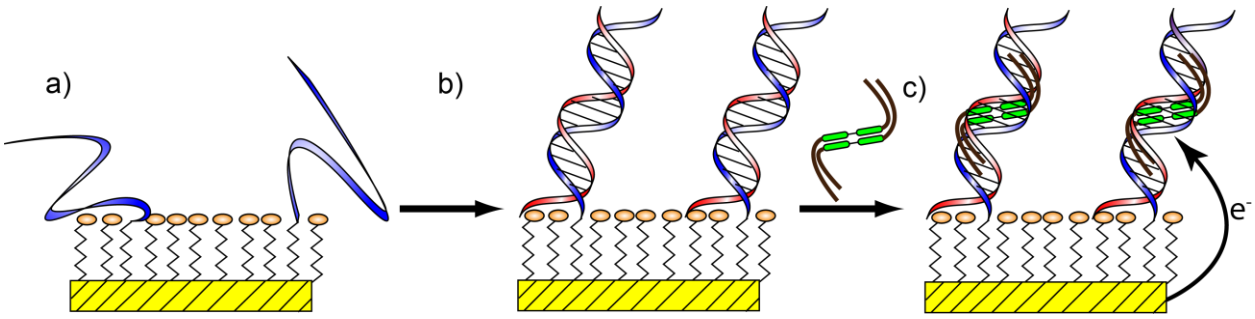

Figure 1.5. Overview of a DNA hybridization sensor. A) ssDNA is immobilized on a Au electrode, followed by passivation of the underlying electrode by mercaptohexanol (orange capped hexane chain). B) dsDNA hybrids are formed on the electrode surface via exposure to the complementary strand. C) dsDNA can be detected using a redox active reporter that binds with some sort of specificity to dsDNA.

A DNA hybridization sensor can be used to easily study individual segments of DNA. This sensor uses single-stranded DNA (ssDNA) immobilized onto the surface of an electrode. This is shown in **Figure 1.5**. Once immobilization of the probe strand is achieved, the ssDNA is hybridized to its complementary target strand, forming a double-stranded DNA duplex (dsDNA)

on the electrode. [30,31,37,38] Redox active molecules can then interact with dsDNA and upon electrochemical oxidation or reduction, produce signals that indicate hybridization. [30,31,39-43] Cationic ruthenium (III) hexamine (RuHex) has been used to detect DNA hybridization based on the doubling of anionic phosphates upon dsDNA formation. [44] Other molecules have been used that exploit certain structural aspects of dsDNA that are not present within ssDNA, such as intercalators that can insert themselves between properly hybridized base pairs and minor groove binders. [39] An example of a sensitive intercalator is methylene blue (MB^+) that can intercalate at distal ends of DNA hybrids immobilized on an electrode surface. Small perturbations in the π-stacking of DNA bases in immobilized oligomers will result in smaller currents, which allow the detection of hybridization, but also mismatches and protein binding. [31,40]

DNA Analysis Using C12-Viologen

One such molecule that has been used effectively to detect DNA hybridization and DNA mismatches is the diviologen derivative, $C_{12}H_{25}V^{2+}C_6H_{12}V^{2+}C_{12}H_{25}$ (V^{2+} is 4,4'-bipyridyl or viologen, referred to as C12-viologen from hereon). C12-viologen features two electroactive viologen units and long hydrophobic chains, and is shown in **Figure 1.6**. The molecule aggregates onto dsDNA, and has been shown with electrochemical and spectroscopic methods to bind within the minor groove of dsDNA. Electrochemically, C12-viologen produces dual wave voltammetry when reduced at approximately -0.5 V vs. Ag/AgCl in the presence of dsDNA, which provides the means to detect hybridization, or discern if DNA is structurally sound. [45] C12-viologen produces dual wave voltammetry when exposed to hybridized dsDNA containing no mismatches. Single wave voltammetry is produced when C12-viologen is exposed to ssDNA as the viologen binds electrostatically to the phosphates. The dual wave indicates that multiple

forms of the viologen exist on dsDNA. After reaching threshold concentrations in the presence of dsDNA, the hydrophobic moieties on the diviologen molecule cause an aggregation of the molecule in the minor groove in addition to the electrostatic binding on the anionic phosphate groups.[45] Upon one-electron reduction, the cation radical viologen groups form dimers in the minor groove location on dsDNA.[45,46] This dimerization is driven by the overlap of the singly occupied π* orbitals within the viologen subunits.

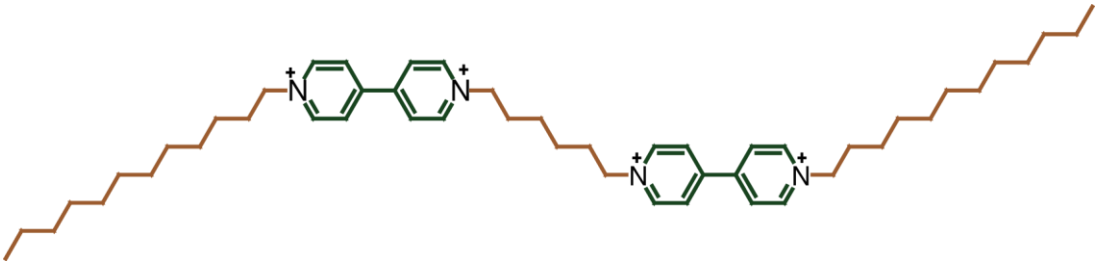

Figure 1.6. C12-viologen structure.

C12-viologen is sensitive to the structure of DNA, and the dual wave voltammetry readily changes in response to structural perturbations within the dsDNA helix that force changes in the binding of C12-viologen, such as mismatches.[46,47] For instance, in DNA-peptide nucleic acid (PNA) duplexes containing mismatches, the altered, mismatched structure forced C12-viologen to change its binding environment in such a way that eliminated the dual wave voltammetry.[8,46] It is this application employing C12-viologen that is exploited to provide a relatively easy way to detect DNA damage and provide DNA structural information.

Sequence Specific DNA Damage Assay

C12-viologen and DNA hybridization have been used previously to detect sequence specific DNA damage from exposure to (±)-*anti*-BPDE.[8,48] A schematic showing how this strategy was employed is shown in **Figure 1.7**. The DNA sequence that was employed was a 21-mer spanning the codon 273 sequence from the TP53 gene. Square wave voltammetry (SWV) was used to show that there were changes at three potentials as the DNA was exposed to BPDE. A background subtracted SWV plot result is shown in **Figure 1.8**. The figure shows the result when the SWV response at t = 0s was subtracted from each timed run. The major finding was that there was a large current increase at approximately -0.38 V, which was consistent with

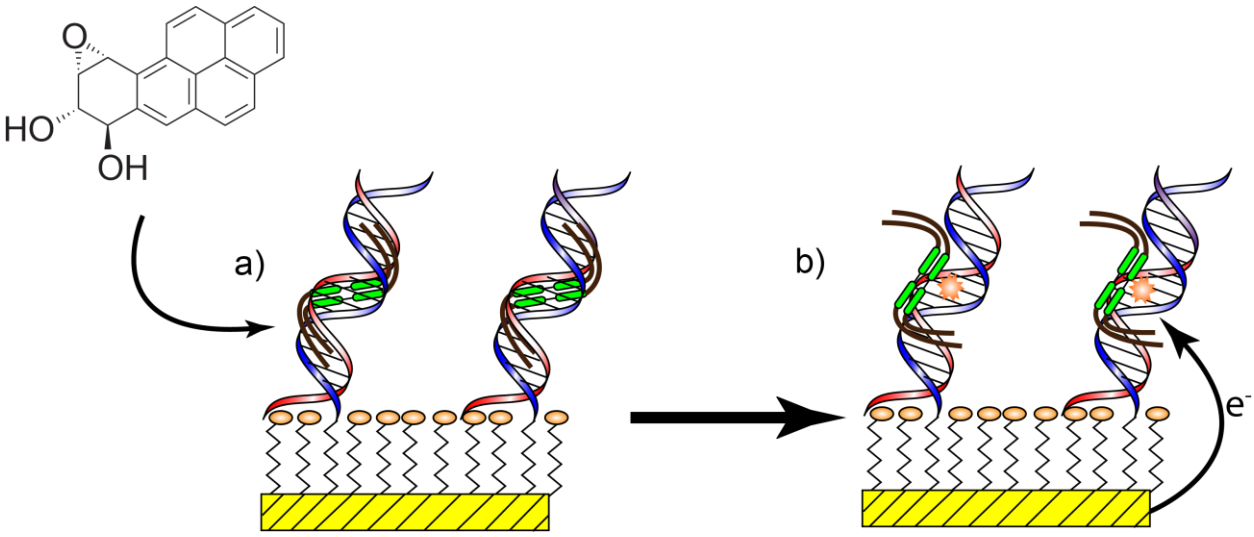

Figure 1.7. DNA damage detection employing a hybridization sensor. A) DNA duplexes are exposed to a xenobiotic (BPDE is shown). The damage will alter the binding of C12-viologen (B), which will change the current response.

the aggregation of C12-viologen on the outside of DNA duplexes. This aggregation was thought to be caused by the presence of hydrophobic BPDE within the minor groove of the duplexes, which is the primary binding location when *anti*-BPDE binds to guanine. Codon 273 is a 5'-CGT-3' sequence, and the guanine within that sequence is thought to be the primary site where the BPDE was bound. Electrochemical controls using DNA without the guanine at that location showed that this was the case.[8] Additionally, mass spectroscopy showed that the DNA oligomers exhibited only a single BPDE adduct. For instance, each oligomer was not adducted by multiple BPDE entities.[8] Wild type (correct sequence) oligomers exhibited much higher amounts of adduction vs. those without the guanine, confirming the electrochemical results.

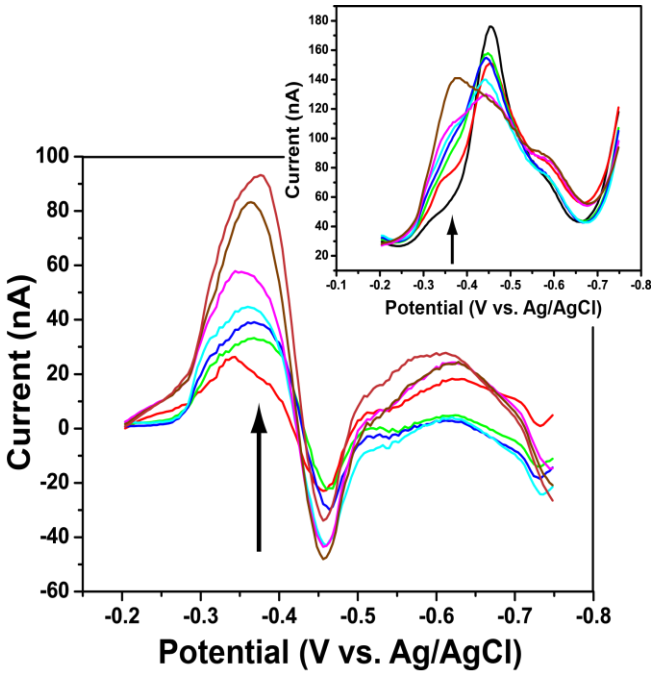

Figure 1.8. Background subtracted current vs. potential square wave voltammogram plots. Inset shows raw data plots where initial (t = 0s) plot was subtracted from all subsequent timed plots (15s – 600s), and the result is what is shown in the main plot. Arrow shows -0.38 V peak.

Epigenetic DNA Methylation and Metabolism Influences

The aforementioned sensor was effective at detecting DNA damage at regular wild type DNA sequences due to exposure to a direct damaging xenobiotic; however, the situation is much more complex in vivo where epigenetic and metabolic processes participate in the genotoxicity process. The goal of this research was to study two different, but related, genotoxicity detection projects. Chapter 3 discusses the first aspect of the research, which focused on studying epigenetic cytosine methylation on the electrochemical sensor response. In addition, the influence of BPDE stereochemistry was explored as well in an effort to understand the electrochemical responses obtained. In vivo, cytosines that are located on the 5' side of guanines are often methylated at the 5-C in the hotspot codons. This changes the hydrophobicity of the dinucleotide sequence and changes how BPDE orients within the duplex when it binds to guanine. Additionally, cytosine methylation influences the eventual adduct structure based on which anti-BPDE enantiomer damages the guanine.

In addition to epigenetic and stereochemical influences, metabolism processes were also studied by introducing model enzymes to the sensor. In Chapter 4, strategies to accomplish this task utilizing myoglobin as a model enzyme are discussed. The overall goal was to generate reactive metabolites *in situ* via metabolism that would then diffuse to the DNA on the electrode, damage the DNA at the reactive codon sites, which could ultimately be detected electrochemically. Myoglobin was employed as it is a convenient heme containing enzyme that can model biological oxidase enzymes under certain conditions. In vivo, cytochrome P450 oxidases metabolize a majority of xenobioitics that are consumed or introduced into the human body. Building on previous results, the electrochemical results show that reactive metabolites

can be detected at a hotspot sequence. The electrochemical responses may provide insight into the stereochemistry of the reaction as well as the ultimate DNA adduct orientation.

Overall, the use of cytosine methylation and enantiomerically pure BPDE has provided clues on how the electrochemical sensor will respond to different adduct orientations, which provides a wealth of powerful information when studying xenobiotic-DNA interactions. The incorporation of enzymes with a DNA hybridization interface has not only allowed the study of how enzymatic processes result in specific reactive metabolites, but it was also opened up new possibilities to utilize more biologically relevant enzymes, such as cytochrome P450s, to study important metabolic related DNA damage processes at specific gene sequences

References

1. Friedberg, E. C. DNA damage and repair. *Nature* **2003**, *421*, 436-440.

2. Schärer, O. D. Chemistry and Biology of DNA Repair. *Angew. Chem. , Int. Ed.* **2003**, *42*, 2946-2974.

3. Boelsterli, U. A. *Mechanistic Toxicology: The Molecular Basis of How Chemicals Disrupt Biological Targets;* Taylor & Francis: Boca Raton, FL, 2007; .

4. Kim, J. H.; Stansbury, K. H.; Walker, N. J.; Trush, M. A.; Strickland, P. T.; Sutter, T. R. Metabolism of benzo[*a*]pyrene and benzo[*a*]pyrene-7,8-diol by human cytochrome P450 1B1. *Carcinogenesis* **1998**, *19*, 1847-1853.

5. Ortiz de Montellano, P. R. *Cytochrome P450: Structure, Mechanism, and Biochemistry;* Kluwer Academic/Plenu: New York, 2005; .

6. Pfeifer, G. P.; Denissenko, M. F.; Oliver, M.; Tretyakova, N.; Hecht, S. S.; Hainaut, P. Tobacco smoke carcinogens, DNA damage and p53 mutations in smoking-associated cancers. *Oncogene* **2002**, *21*, 7435-7451.

7. Denissenko, M. F.; Pao, A.; Tang, M.; Pfeifer, G. P. Preferential Formation of Benzo[*a*]pyrene Adducts at Lung Cancer Mutational Hotspots in *P53*. *Science* **1996**, *274*, 430-432.

8. Satterwhite, J. E.; Pugh, A. M.; Danell, A. S.; Hvastkovs, E. G. Electrochemical Detection of *anti*-Benzo[*a*]pyrene Diol Epoxide DNA Damage on *TP53* Codon 273 Oligomers. *Anal. Chem.* **2011**, *83*, 3327-3335.

9. Pfeifer, G. P.; Besaratinia, A. Mutational spectra of human cancer. *Hum. Genet.* **2009**, *125*, 493-506.

10. Giono, L. E.; Manfredi, J. J. The p53 Tumor Suppressor Participates in Multiple Cell Cycle Checkpoints. *J. Cell. Physiol.* **2006**, *209*, 13-20.

11. Vogelstein, B.; Lane, D.; Levine, A. J. Surfing the p53 network. *Nature* **2000**, *408*, 307-310.

12. Vogelstein, B.; Kinzler, K. W. Cancer genes and the pathways they control. *Nat. Med.* **2004**, *10*, 789-799.

13. Vousden, K. H.; Lu, X. Live or let die: the cell's response to p53. *Nat. Rev. Cancer* **2002**, *2*, 594-604.

14. Vousden, K. H.; Lane, D. P. P53 in health and disease. *Nature* **2007**, *8*, 275-283.

15. Bullock, A. N.; Fersht, A. R. Rescuing the function of mutant p53. *Nat. Rev. Cancer* **2001**, *1*, 68-76.

16. Smith, L. E.; Denissenko, M. F.; Bennett, W. P.; Li, H.; Amin, S.; Tang, M.; Pfeifer, G. P. Targeting of Lung Cancer Mutational Hotspots by Polycyclic Aromatic Hydrocarbons. *J. Natl. Cancer Inst.* **2000**, *92*, 803-811.

17. Geacintov, N. E.; Cosman, M.; Hingerty, B. E.; Amin, S.; Broyde, S.; Patel, D. J. NMR Solution Structures of Stereoisomeric Covalent Polycyclic Aromatic Carcinogen– DNA Adducts: Principles, Patterns, and Diversity. *Chem. Res. Toxicol.* **1997**, *10*, 111-146.

18. Satterwhite, J. E. Electrochemical Detection of Benzo[*a*]pyrene Metabolite DNA Damage: Implications of Nucleobase Sequence and Adduct Stereochemistry. M.S. Thesis, East Carolina University, Greenville, NC, 2011.

19. Pradhan, P.; Gräslund, A.; Seidel, A.; Jernström, B. Implications of Cytosine Methylation on (+)-*anti*-Benzo[*a*]pyrene 7,8-Dihydrodiol 9,10-Epoxide N^2-dG Adduct Formation in 5'-d(CGT), 5'-d(CGA), and 5'-d(CGC) Sequence Contexts of Single- and Double- Stranded Oligonucleotides. *Chem. Res. Toxicol.* **1999**, *12*, 816-821.

20. Denissenko, M. F.; Chen, J. X.; Tang, M.; Pfeifer, G. P. Cytosine methylation determines hot spots of DNA damage in the human *P53* gene. *Proc. Natl. Acad. Sci. U. S. A.* **1997**, *94*, 3893-3898.

21. Zhang, N.; Lin, C.; Huang, X.; Kolbanovskiy, A.; Hingerty, B.; Amin, S.; Broyde, S.; Geacintov, N. E.; Patel, D. J. Methylation of Cytosine at C5 in a CpG Sequence Context Causes a Conformational Switch of a Benzo[*a*]pyrene diol epoxide-N^2-guanine Adduct in DNA from a Minor Groove Alignment to Interacalation with Base Displacement. *J. Mol. Biol.* **2005**, *346*, 951-965.

22. Chen, Z. X.; Riggs, A. D. DNA Methylation and Demethylation in Mammals. *J. Biol. Chem* **2011**, *286*, 18347-18353.

23. Tornaletti, S.; Pfeifer, G. P. Complete and tissue-independent methylation of CpG sites in the p53 gene: implications for mutations in human cancers. *Oncogene* **1995**, *10*, 1493-1499.

24. Chen, J. X.; Zheng, Y.; West, M.; Tang, M. Carcinogens Preferentially Bind at Methylated CpG in the p53 Mutational Hot Spots. *Cancer Res.* **1998**, *58*, 2070-2075.

25. Denissenko, M. F.; Pao, A.; Pfeifer, G. P.; Tang, M. Slow repair of bulky DNA adducts along the nontranscribed strand of the human *p53* gene may explain the strand bias of transversion mutations in cancers. *Oncogene* **1998**, *16*, 1241-1247.

26. Feng, Z.; Hu, W.; Rom, W. N.; Beland, F. A.; Tang, M. 4-Aminobiphenyl is a major etiological agent of human bladder cancer: eveidence from its DNA binding spectrum in human *p53* gene. *Carcinogenesis* **2002**, *23*, 1721-1727.

27. Feng, Z.; Hu, W.; Hu, Y.; Tang, M. Acrolein is a major cigarette-related lung cancer agent: Preferential binding at *p53* mutational hotspots and inhibition of DNA repair. *Proc. Natl. Acad. Sci. U. S. A.* **2006**, *103*, 15404-15409.

28. Pfeifer, G. P.; Riggs, A. D. Genomic Sequencing by Ligation-Mediated PCR. *Mol. Biotechnol.* **1996**, *5*, 281-288.

29. Pfeifer, G. P.; Denissenko, M. F.; Tang, M. PCR-based approaches to adduct analysis. *Toxicol. Lett.* **1998**, *102-103*, 447-451.

30. Odenthal, K. J.; Gooding, J. J. An introduction to electrochemical DNA biosensors. *Analyst* **2007**, *132*, 603-610.

31. Drummond, T. G.; Hill, M. G.; Barton, J. K. Electrochemical DNA sensors. *Nat. Biotechnol.* **2003**, *21*, 1192-1199.

32. Paleček, E.; Fojta, M.; Tomschik, M.; Wang, J. Electrochemical biosensors for DNA hybridization and DNA damage. *Biosens. Bioelectron.* **1998**, *13*, 621-628.

33. Hvastkovs, E. G.; So, M.; Krishnan, S.; Bajrami, B.; Tarun, M.; Jansson, I.; Schenkman, J. B.; Rusling, J. F. Electrochemiluminescent Arrays for Cytochrome P450-Activated Genotoxicity Screening. DNA Damage from Benzo[*a*]pyrene Metabolites. *Anal. Chem.* **2007**, *79*, 1897-1906.

34. Krishnan, S.; Hvastkovs, E. G.; Bajrami, B.; Choudhary, D.; Schenkman, J. B.; Rusling, J. F. Synergistic Metabolic Toxicity Screening Using Microsome/DNA Electrochemiluminescent Arrays and Nanoreactors. *Anal. Chem.* **2008**, *80*, 5279-5285.

35. Lee, M.; Kumar, R. A.; Sukumaran, S. M.; Hogg, M. G.; Clark, D. S.; Dordick, J. S. Three-dimensional cellular microarray for high-throughput toxicology assays. *Proc. Natl. Acad. Sci. U. S. A.* **2008**, *105*, 59-63.

36. Rusling, J. F.; Hvastkovs, E. G.; Hull, D. O.; Schenkman, J. B. Biochemical applications of ultrathin films of enzymes, polyions and DNA. *Chem. Commun.* **2008**, 141-154.

37. Lucarelli, F.; Marrazza, G.; Turner, A. P.; Mascini, M. Carbon and gold electrodes as electrochemical transducers for DNA hybridisation sensors. *Biosens. Bioelectron.* **2004**, *19*, 515-530.

38. Pividori, M. I.; Alegret, M. S. Electrochemical genosensor design; immobilisation of oligonucleotides onto transducer surfaces and detection methods. *Biosens. Bioelectron.* **2000**, *15*, 291-303.

39. Hvastkovs, E. G.; Buttry, D. A. Recent advances in electrochemical DNA hybridization sensors. *Analyst* **2010**, *135*, 1817-1829.

40. Boon, E. M.; Jackson, N. M.; Wightman, M. D.; Kelley, S. O.; Hill, M. G.; Barton, J. K. Intercalative Stacking: A Critical Feature of DNA Charge-Transport Electrochemistry. *J. Phys. Chem. B* **2003**, *107*, 11805-11812.

41. Jackson, B. A.; Barton, J. K. Recognition of DNA Base Mismatches by a Rhodium Intercalator. *J. Am. Chem. Soc.* **1997**, *119*, 12986-12987.

42. Wong, E. L. S.; Gooding, J. J. Charge Transfer through DNA: A Selective Electrochemical DNA Biosensor. *Anal. Chem.* **2006**, *78*, 2138-2144.

43. Wong, E. L. S.; Gooding, J. J. The Electrochemical Monitoring of the Perturbation of Charge Transfer through DNA by Cisplatin. *J. Am. Chem. Soc.* **2007**, *129*, 8950-8951.

44. Steel, A. B.; Herne, T. M.; Tarlov, M. J. Electrochemical Quantification of DNA Immobilized on Gold. *Anal. Chem.* **1998**, *70*, 4670-4677.

45. Hvastkovs, E. G.; Buttry, D. A. Minor Groove Binding of a Novel Tetracationic Diviologen. *Langmuir* **2006**, *22*, 10821-10829.

46. Hvastkovs, E. G.; Buttry, D. A. Characterization of Mismatched DNA Hybridization via a Redox-Active Diviologen Bound in the PNA−DNA Minor Groove. *Langmuir* **2009**, *25*, 3839-3844.

47. Hvastkovs, E. G.; Buttry, D. A. Electrochemical Detection of DNA Hybridization via Bis-Intercalatoin of Naphthylimide-Functionalized Viologen Dimer. *Anal. Chem.* **2007**, *79*, 6922-6926.

48. Satterwhite, J. E.; Trumbo, C. M.; Danell, A. S.; Hvastkovs, E. G. Electrochemical Study on the Effects of Epigenetic Cytosine Methylatoin on *Anti*-Benzo[*a*]pyrene Diol Epoxide Damage at TP53 Oligomers. *Anal. Chem.* **2013**, *85*, 1183-1191.

CHAPTER 2: MATERIALS, INSTRUMENTATION, AND METHODS

Materials

DNA oligomer sequences used in these studies are listed in **Table 2.1** and were purchased from IDT DNA Technologies (Coralville, IA).

Table 2.1. DNA oligomer names and their corresponding 21-mer oligomer DNA sequence spanning codons 270-276 with codons of interest bolded.

Name of Sequence	**Specific Sequence**
wtP.273	HS – 5' – TTT GAG GTG **CGT** GTT TGT GCC – 3'
wtC.273	5' – GGC ACA AAC ACG CAC CTC AAA – 3'
meP.273	HS – 5' – TTT GAG GTG ^{me}**CGT** GTT TGT GCC – 3'
meC.273	5' – GGC ACA AAC A^{me}CG CAC CTC AAA – 3'
conP.273	HS – 5' – TTT GAG GTG **CCT** GTT TGT GCC – 3'
conC.273	5' – GGC ACA AAC AGG CAC CTC AAA – 3'

Sequences symbolized with a P denote ssDNA probe (nontranscribed, coding) strands that were immobilized onto the surface of the electrode. Sequences symbolized with a C are complementary target (noncoding) strands that were used to hybridize to probe strands, forming dsDNA hybrids.

Benzo[*a*]pyrene-7,8-dihydrodiol-9,10-epoxide, (±)-*anti*-BPDE and (+)-*anti*-BPDE were obtained from Midwest Research Institute NCI Chemical Carcinogen Reference Standards Repository (Kansas City, MO). Benzo[*a*]pyrene (BP), Mercaptohexanol (MCH), Tris(hydroxymethyl) aminomethane hydrochloride (Tris-HCl), Tris(hydroxymethyl)

aminomethane (Tris base), monopotassium phosphate (KH_2PO_4), dipotassium phosphate (K_2HPO_4), and tetrahydrofuran (THF) were obtained from Sigma Aldrich. All other chemicals were reagent grade and used as received.

Instrumentation

All electrochemical measurements were performed on a CH Instruments 660A workstation (Austin, TX). A 2 mm diameter gold (Au) disk working electrode was connected to the potentiostat and placed in an electrochemical cell along with a saturated Ag/AgCl (Saturated KCl) reference electrode and a platinum wire (Pt) counter electrode. The Au and Ag/AgCl electrodes used in this study were purchased from CH Instruments (Austin, TX).

A Nanodrop 2000c Spectrophotometer (Thermo Scientific) was used to confirm DNA oligomer concentrations. A Varian Cary 300 Bio UV-Vis Spectrophotometer was used to quantify BPDE concentration in order to determine the amount to use during damage experiments for appropriate BPDE concentration. The concentration of BPDE (dissolved in THF) was determined by measuring the absorbance at 346 nm in a 1.0-cm path length quartz cuvette. THF alone was employed as the blank. The molar absorptivity coefficient of BPDE was previously determined to be 48770 M^{-1} cm^{-1}.[1]

Methods

Buffers

The buffers made and used in this work are listed in **Table 2.2** below.

Table 2.2. List of buffers used during experimental procedures with each of their corresponding contents and pH level.

Name	Abbreviation	Contents	pH
Electrochemical Buffer	E-Buffer	10mM Tris 10 mM NaCl	7.4
Hybridization Buffer		10 mM Tris 1 mM EDTA 1 M NaCl	7.4
Immobilization Buffer		1 M Phosphate ($H_2PO_4^-/HPO_4^{2-}$) 1 mM EDTA	7.4
Tris-EDTA Buffer	TE Buffer	10 mM Tris 1 mM EDTA	8.0
Phosphate Buffer		500 mM or 50 mM Phosphate ($H_2PO_4^-/HPO_4^{2-}$)	7.4 or 8.0
0.5% w/v Polyethylene Glycol Solution	PEG Solution	0.5% w/v Polyethylene Glycol 50 mM Phosphate Buffer pH 8.0	8.0

BPDE Preparation

BPDE is a known carcinogen and was handled using proper personal protective equipment. BPDE was distributed into amber vials under a N_2 atmosphere due to its sensitivity to moisture and light. Vials were kept sealed at – 20°C prior to use. A fresh 1-2 mM BPDE stock solution was prepared in an amber vial by dissolving BPDE in THF for each experiment.

BP Preparation

A fresh BP stock solution was made in THF for each experiment. Approximately 2 mg of BP was dissolved in THF for an approximately 0.04 M solution. The solution was then diluted into an amber vial to 1 mM in THF and stored – 20°C between uses.

Myoglobin Preparation

Purchased myoglobin (Mb) was stored at – 20°C until needed. After allowing the Mb to equilibrate to room temperature for 20 minutes, approximately 20 mg of Mb was dissolved in 5 mL of 50 mM phosphate buffer. The mixture was then centrifuged at 15,000 x g for 40 minutes using an Amicon Ultra 30K MW cutoff centrifugal filter device. After centrifugation, the filtered solution was transferred into a vial and stored at 4°C between uses. This procedure produced approximately 3 mg/mL Mb solution.

NADPH Preparation

A fresh NADPH stock solution was made for each experiment. Between 0.5 mg – 1.0 mg of NADPH was dissolved in 50 mM phosphate buffer. The solution was then diluted to an appropriate concentration in 50 mM phosphate buffer.

Synthesis of C12-Viologen

$C_{12}H_{25}V^{2+}C_6H_{12}V^{2+}C_{12}H_{25}$ (V^{2+} = 4,4'-bipyridyl or viologen, the full molecule is referred to as C12-viologen from here on) was previously synthesized following a previously established protocol. [2,3]

DNA Preparation for Electrochemical Experiments

ssDNA probe oligomer sequences were purchased with a 5'-thiol modification. Thiolated oligomers were shipped as disulfides for stability. In order to reduce disulfide bonds, 100 µL of 2% triethylamine (TEA) and 50 mM dithiothreitol (DTT) was added to the DNA oligomer. The solution was left to stand at room temperature for 10 minutes, and then 500 µL of acetone containing 2% lithium perchlorate ($LiClO_4$) w/w was added to the solution. The solution was then cooled to – 20.0°C for 15 min. Following this, the solution was centrifuged at 5000 RPM for 5 min. After centrifugation, the supernatant was removed, and the DNA pellet was dried with argon (Ar) gas. Probe oligomer sequences were then diluted to 1 mM in TE buffer, followed by dilution to 20 µM in immobilization buffer.

Complementary oligomers were purchased unmodified. Complementary oligomers were immediately diluted to 1 mM in TE buffer, followed by dilution to 2.0 µM in hybridization buffer. All aqueous solutions were made with 18 mΩ · cm deionized water (DI H_2O). All DNA was stored at – 20°C prior to use. [2-5]

Electrode Preparation

Au electrodes (2 mm, CH Instruments) were cleaned before the start of DNA experiments following a previously established protocol.[2-5] In order to ensure that the Au surfaces were cleared of any adsorbed material and also to ensure that the electrodes functioned properly, the electrodes were cleaned by immersion in piranha solution (2:1 volume concentrated H_2SO_4 to 30-35% H_2O_2). After sitting in the solution for 5 to 10 minutes, the electrodes were rinsed with ethanol and DI H_2O. The electrodes were then sequentially polished with 1.0 μm, 0.3 μm, and 0.05 μm diameter alumina particles on a polishing pad (Buehler). A slurry was made by wetting the area with DI H_2O for each consecutive alumina diameter polish. Electrodes were moved in a "figure eight" motion through each respective slurry mixture for 1 minute 30 seconds each. Electrodes were rinsed with DI H_2O after each cycle of polishing. Following the rinsing, electrodes were briefly sonicated in DI H_2O as to remove any residual alumina. Electrodes were then placed in 10 mL of 0.5 M H_2SO_4 and electrochemically cleaned by cycling from +0.1 V to +1.75 V at 0.25 V/s for approximately 10 min. Following the cleaning cycle, a quantification cycle was obtained by cycling from +0.1 V to +1.45 V at 0.25 V/s to measure the electroactive surface area. The actual surface area of the electrode was calculated by integration of the Au-oxide stripping peak in the tenth reduction scan of the quantification cycle. The current was converted to surface area using the conversion factor 386 μC cm^{-2}.[6] Usually, this resulted in a surface area of 0.04 cm^2 to 0.05 cm^2 and a surface roughness factor of 1.3 to 1.6 (calculated as actual surface area/geometrical surface area). The clean electrode was rinsed with ethanol and dried using a stream of Ar gas.

DNA Immobilization

An aliquot of 20 µM thiolated probe DNA was exposed to a clean gold electrode for 30 to 90 seconds. The electrode was then rinsed with DI H_2O followed by immersion in 5 µM mercaptohexanol (MCH) in DI H_2O for 45 minutes. After MCH exposure, the electrode was again rinsed with DI H_2O followed by exposure to the complementary strand (2 µM in hybridization buffer) for 2 hours at 37.0°C to form dsDNA. After exposure to the complementary strand, the electrode was rinsed with E-buffer followed by immersion in E-buffer for 30 minutes at 37.0°C to remove non-specifically bound DNA. Electrodes were then immediately stored at 4°C until used. [2-5,7,8]

Electrochemical Measurements

Cyclic voltammetry (CV), chronocoulometry (CC), and square wave voltammetry (SWV) were all used in this study to perform electrochemical measurements. Voltammetry parameters for different experimental conditions were as follows:

Table 2.3. Electrochemical parameters for quantification of immobilized DNA.

	Cyclic Voltammetry (CV)	**Chronocoulometry (CC)**
Initial E	0 V	0 V
High E	0 V	N/A
Low E	-0.4 V	N/A
Final E	0 V	-0.4 V
Scan Rate	0.1 V/s	N/A
Sweep Segments	4	N/A
Sample Interval	0.001 V	0.00025 s
Pulse Width	N/A	0.1 s
Number of Steps	N/A	1

Table 2.4. Electrochemical parameters for detection of C12-viologen and monitoring of DNA damage from different xenobiotic solutions.

	Cyclic Voltammetry (CV)	**Square Wave Voltammetry (SWV)**
Initial E	0 V	-0.20 V
High E	0 V	N/A
Low E	-0.7 V	N/A
Final E	0 V	-0.75 V
Scan Rate	0.1 V/s	N/A
Sweep Segments	4	N/A
Sample Interval	0.001 V	N/A
Increase E Steps	N/A	0.004 V
Amplitude	N/A	0.025 V
Frequency	N/A	2 Hz

All measurements were performed with a sensitivity of 1.00×10^{-6} A/V.

Quantification of Immobilized DNA

The amount of ssDNA and dsDNA were quantified separately using a cationic redox molecule, ruthenium hexamine ($Ru(NH_3)_6)^{2+/3+}$, RuHex), that electrostatically binds to the DNA phosphate backbone. [2-5,7,9] Chronocoulometry (CC) was used to quantify the amount of RuHex adsorbed on the DNA-modified electrode. [10] Essentially, CC measures the charge (Q) associated with an electroactive process, which can be simplified to include charge arising from three components: the diffusion of electroactive species, double layer charging based on the movement of ions in solution, and charge from surface adsorbed species. This is summarized in **Equation 2.1** below:

$$\mathbf{Q = Q_{diff} + Q_{dl} + Q_{surf}} \qquad \mathbf{2.1}$$

Surface bound charge is the only component of interest, as this charge is directly proportional to the amount of DNA present on the electrode surface. Therefore, CC experiments are performed in such a way to subtract out charge arising from diffusion and double layer charging by first performing a blank scan with no RuHex present and subtracting this charge out from subsequent scans. Therefore, the charge obtained from scans containing RuHex is then attributed to that bound at the surface of the electrode.[7] This charge is directly proportional to the amount of bound RuHex shown in **Equation 2.2** as follows:

$$\mathbf{Q = nFA\Gamma_0} \qquad \mathbf{2.2}$$

Where n is the number of electrons per molecule for reduction (1 in this case), F is Faraday's constant (9.65 x 10^4 C/mol e^-), A is the electrode area (cm^2), and Γ_0 is the amount of RuHex bound at the electrode surface (mol/cm^2). **Equation 2.3** gives the relationship between the surface density of RuHex and DNA on the electrode.[2,7]

$$\mathbf{\Gamma_{DNA} = \Gamma_0 \left(\frac{z}{m}\right) (N_A)} \qquad \mathbf{2.3}$$

Where Γ_{DNA} is the DNA probe surface density ($molecules/cm^2$), m is the number of bases in the DNA, which varied depending on whether ssDNA or dsDNA was being quantified (21 vs. 42 bases), z is the charge of the redox molecule (3+), and N_A is Avogadro's number. Using this quantification method, the surface density of dsDNA (Γ_{DNA}) was typically found to be ~1.8-2.5 x

10^{12} molecules/cm^2. After determining the surface density, electrodes were immersed in 2 M NaCl to remove the RuHex electrostatically bound to the DNA phosphate backbone. After sitting in NaCl for 2 minutes, the electrodes were rinsed with E-buffer.

Addition of C12-Viologen to Electrochemical Cell

Between 0.5 mg – 0.9 mg of C12-viologen was added to 5 mL of E-buffer in order to prepare a C12-viologen stock solution. The solution was then heated to 45.0°C to solubilize the C12-viologen. C12-viologen was then added to the electrochemical cell for a final concentration of 7 μM to 10 μM. This concentration varied depending on what was seen in the cyclic voltammetric analysis (see below, DNA Damage with BPDE). Typically, a dual wave CV was desired, and this was achieved at approximately 10 μM C12-viologen concentration in the E-buffer.

DNA Damage with BPDE

Electrodes containing immobilized dsDNA were placed in an electrochemical cell containing 10 mL of E-buffer. SWV and CV measurements were initially used to achieve a dual wave voltammogram, which ensured sufficient C12-viologen concentration in the E-buffer and served as a convenient qualitative monitor for dsDNA coverage on the electrode. These scans, before any damage to the electrode had taken place, were set as baseline, or t = 0s exposure. Next, changes in C12-viologen-DNA binding as a function of exposure to racemic (±)-*anti*-BPDE or enantiomerically pure (+)-*anti*-BPDE were recorded. The electrodes were removed from the electrochemical cell and exposed to a 50 μL reaction mixture containing a desired concentration of (±)-*anti*-BPDE or (+)-*anti*-BPDE in E-buffer for increasing times from 15

seconds to 600 seconds at 37°C. After each time period, the electrode was rinsed with E-buffer and placed back into the electrochemical cell for voltammetric analysis. The electrochemical cell was purged with Ar gas for 5 minutes prior to voltammetric analysis to remove any oxygen from the cell.

DNA Damage from a Bioactivation Process Using Myoglobin

Electrodes containing immobilized dsDNA (wtP-wtC.273 also known as wt.273) were placed in an electrochemical cell containing 10 mL of E-buffer. The same parameters and electrodes outlined previously were used.

For solution phase Mb-BP damage experiments, after the baseline measurements were taken, electrodes were exposed to a 50 µL reaction mixture containing varying concentrations of BP, 250 nM hydrogen peroxide (H_2O_2), and 3 mg/mL Mb in 50 mM phosphate buffer for increasing times from 15 seconds to 600 seconds at 37°C, in order to determine the optimal concentration of BP. After each time period, the electrode was rinsed with PEG solution or E-buffer and placed back into the electrochemical cell, purged with Ar gas, and voltammetric measurements taken.

Mb experiments were also performed by adsorbing the enzyme onto the surface of the dsDNA modified electrode. This process was essentially a presaturation of Mb on the electrode before damage experiments were performed. After dsDNA formation, Mb (3 mg/mL, 50 mM phosphate buffer pH 7.4) was then allowed to adsorb on the electrode surface for approximately 40-60 minutes. The saturation was confirmed by taking scans in the C12-viologen E-buffer to ensure that electrochemical signals stabilized before damage experiments. Once the current stabilized, the electrodes were then exposed to a 50 µL reaction mixture containing varying

concentrations of BP and 250 nM H_2O_2 in 50 mM phosphate buffer. Electrodes were rinsed in E-buffer before being placed back into electrochemical cell for voltammetric analysis.

DNA Damage from a Bioactivation Process Using Cytochrome P450

Electrodes containing immobilized dsDNA (wt.273) were also presaturated with cyt P450 enzymes following a similar protocol. After formation of dsDNA, the electrodes were then exposed to a lysed DH5α *E. coli* membrane fraction aliquot containing cytochrome (cyt) P450 1A1 or 1A2 and cytochrome P450 reductase (CPR).[11] The enzyme mixture was allowed to adsorb onto the electrode surface for approximately 40-60 minutes. Similar protocols ensuring saturation were followed. The electrode was then exposed to a 50 µL reaction mixture containing varying concentrations of BP and NADPH in 50 mM phosphate buffer for increasing times from 15 seconds to 600 seconds at 37°C. After each time period, the electrode was rinsed with E-buffer and placed back into the electrochemical cell, and purged with Ar gas before voltammetric analysis.

Data Analysis

Voltammetric data was obtained with CH Instruments software. Files were saved as .txt and imported into Microsoft Excel for grouping. The Excel file was then imported into OriginPro8 graphing software. SWV data was background corrected by subtracting the baseline (0 s) from each exposure plot. The baseline for all experiments was taken as the first SWV before any exposure to BP or BPDE.

References

1. MacLeod, M. C.; Tang, M. Interactions of Benzo[a]pyrene diol-epoxides with linear and supercoiled DNA. *Cancer Res.* **1985**, *45*, 51-56.

2. Satterwhite, J. E. Electrochemical Detection of Benzo[*a*]pyrene Metabolite DNA Damage: Implications of Nucleobase Sequence and Adduct Stereochemistry. M.S. Thesis, East Carolina University, Greenville, NC, 2011.

3. Hvastkovs, E. G.; Buttry, D. A. Minor Groove Binding of a Novel Tetracationic Diviologen. *Langmuir* **2006**, *22*, 10821-10829.

4. Satterwhite, J. E.; Pugh, A. M.; Danell, A. S.; Hvastkovs, E. G. Electrochemical Detection of *anti*-Benzo[*a*]pyrene Diol Epoxide DNA Damage on *TP53* Codon 273 Oligomers. *Anal. Chem.* **2011**, *83*, 3327-3335.

5. Satterwhite, J. E.; Trumbo, C. M.; Danell, A. S.; Hvastkovs, E. G. Electrochemical Study on the Effects of Epigenetic Cytosine Methylatoin on *Anti*-Benzo[*a*]pyrene Diol Epoxide Damage at TP53 Oligomers. *Anal. Chem.* **2013**, *85*, 1183-1191.

6. Bard, A. J.; Faulkner, L. R. In Wiley: New York, 2001; .

7. Steel, A. B.; Herne, T. M.; Tarlov, M. J. Electrochemical Quantification of DNA Immobilized on Gold. *Anal. Chem.* **1998**, *70*, 4670-4677.

8. Herne, T. M.; Tarlov, M. J. Characterization of DNA Probes Immobilized on Gold Surfaces. *J. Am. Chem. Soc.* **1997**, *119*, 8916-8920.

9. Odenthal, K. J.; Gooding, J. J. An introduction to electrochemical DNA biosensors. *Analyst* **2007**, *132*, 603-610.

10. Heineman, W. R.; Kissinger, P. T. In *Large-Amplitude Controlled-Potential Techniques;* Kissinger, P. T., Heineman, W. R., Eds.; Laboratory Techniques in Electroanalytical Chemistry; Marcel Dekker, Inc.: New York, NY, 1996; pp 51-125.

11. Hvastkovs, E. G.; Schenkman, J. B.; Rusling, J. F. Metabolic Toxicity Screeing Using Electrochemiluminescence Arrays Coupled with Ezyme – DNA Biocolloid Reactors and Liquid Chromatography – Mass Spectrometry. *Annu. Rev. Anal. Chem.* **2012**, *5*, 79-105.

CHAPTER 3: ELECTROCHEMICAL STUDY ON THE EFFECTS OF EPIGENETIC CYTOSINE METHYLATION ON *ANTI*-BENZO[*A*]PYRENE DIOL EPOXIDE DAMAGE AT TP53 OLIGOMERS

Portions of the following have been reprinted with permission from Satterwhite, J. E.; Trumbo, C. M.; Danell, A. S.; Hvastkovs, E. G. Electrochemical Study on the Effects of Epigenetic Cytosine Methylation on *Anti*-Benzo[*a*]pyrene Diol Epoxide Damage at TP53 Oligomers. *Anal. Chem.* **2013**, 85, 1183-1191.

Results

Our group has previously shown that electrochemical DNA hybridization sensors can be used to study genetic hotspots. Electrodes modified with dsDNA were exposed to BPDE to study the effect of BPDE exposure at an oligomer containing hotspot codon 273. DNA damage was detected electrochemically using C12-viologen. C12-viologen reduction in the presence of damaged DNA resulted in increases in current at different potentials. Changes at these potentials suggested changes in the environment in which C12-viologen was bound to DNA. These changes were based on how BPDE altered the DNA structure. The C12-viologen population that exhibited a positive potential shift from the formal reduction potential indicated that the oxidized C12-viologen was actually in a lower stability environment compared to when no DNA damage had taken place. This was consistent with C12-viologen bound external to the helix, which was due to bulky BPDE adducts residing in the minor groove of the DNA. (±)-*anti*-BPDE has been shown to bind in this manner on wild type DNA, or DNA without any epigenetic changes such as cytosine methylation. Control experiments showed that the C12-viologen current increases were much more prevalent when BPDE could damage the codon 273 guanine, which provided the evidence to support site-specific DNA damage detection. Overall, C12-viologen was shown to provide a relatively easy way to detect sequence specific DNA as well as provide DNA structural information. [1-4]

To build on this previous work, epigenetic modifications to the DNA were studied. Gold electrodes were modified with methylated 21-mer oligomer DNA sequence, spanning codons 270-276 of the TP53 gene, which contained the hotspot codon 273. Cytosines located 5' to guanine at the codon 273 site were methylated at the 5-carbon (5-meC). Methylation was on the immobilized probe strand (meP-wtC.273), hybridized complementary strand (wtP-meC.273), or both strands (meP-meC.273). 5-C methylation produces a hydrophobic methyl group that protrudes into the major groove of the double helix.[5] Initially racemic (±)-*anti*-BPDE was used to damage the DNA.

(±)-*anti*-BPDE Exposure

During initial studies, 200 µM (±)-*anti*-BPDE was exposed to the meP-meC.273 sequence for increasing time periods up to 600 s. **Figure 3.1** shows the background subtracted SWV as (±)-*anti*-BPDE was exposed to the DNA.

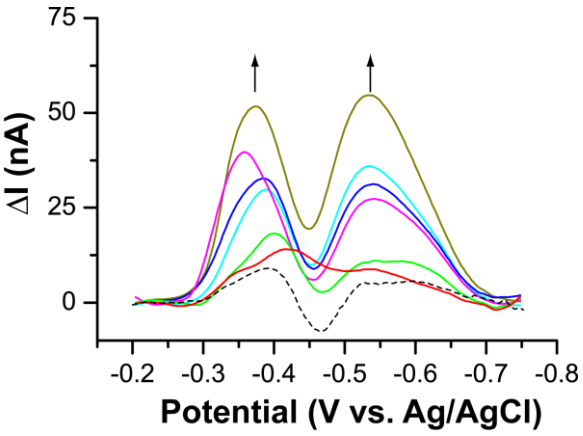

Figure 3.1. Background-subtracted SWV response showing C12-viologen reduction at meP-meC.273 exposed to 200 µM (±)-*anti*-BPDE for 15 s (red), 30 s (green), 60 s (light blue), 180 s (dark blue), 300 s (pink), and 600 s (dark yellow). Black dash shows response after exposure to 200 µM benzo[*a*]pyrene for 600 s.

Figure 3.1 also features a control showing the negligible current response from exposure to 200 μM benzo[*a*]pyrene, suggesting that the current increases are due to the BP metabolite adducting the DNA, rather than a benzo[*a*]pyrene intercalative noncovalent interaction. This response is consistent with previous data showing that BPDE and not BP exposure caused the current increases. BP intercalates between base pairs and causes a lengthening of the helix, but does not covalently adduct the DNA. BPDE covalently adducts DNA, primarily guanine, and resides at different locations along the DNA helix, causing the C12-viologen to change its binding environment, leading to the changes in current at the -0.4 and -0.55 V potentials (arrows in **Figure 3.1**).

Figure 3.2 shows that the C12-viologen response at meP-meC.273 (red) is much different then at the nonmethylated, wild type sequence (wtP-wtC.273, black) when exposed to (±)-*anti*-BPDE. The two arrows denote the two potentials where current change is most prominent. **Figure 3.2** illustrates that cytosine methylation alters the C12-viologen voltammetric response as compared to the non-methylated sequence. Unlike the response for wt.273 where the primary current response was at -0.38 V with negligible current increase at -0.55 V, the response for meP-meC.273 shows significant peak growth at both -0.38 V and -0.55 V, while producing lower overall peak intensity at -0.38 V compared to response under non-methylated conditions. The large peak intensity at -0.55 V indicates that oxidized C12-viologen binds within a more stable environment on the DNA as BPDE is exposed to the dual 5-meC containing hybrid. This higher stability environment is consistent with C12-viologen binding in the minor groove.

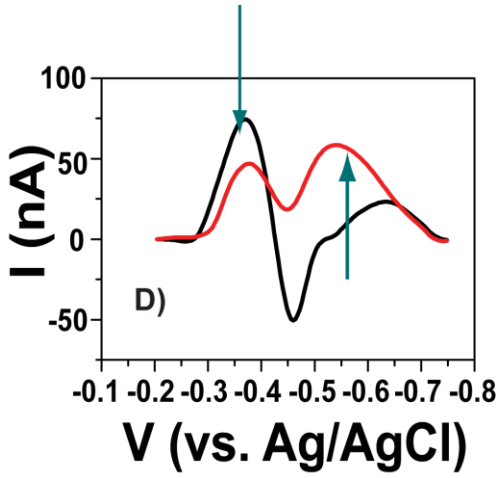

Figure 3.2. Background-subtracted SWV response showing C12-viologen reduction at wt.273 (black) and meP-meC.273 (red) exposed to 200 µM (±)-*anti*-BPDE for 300 s.

(+)-*anti*-BPDE Exposure

To further understand the cause of the different current responses when methylated oligomers were employed, enantiomerically pure (+)-*anti*-BPDE was exposed to fully methylated (both probe and complement strand) and partially methylated oligomers (either strand containing a 5-meC) immobilized on the gold electrode. **Figure 3.3** shows the background subtracted SWV response when 100 µM (+)-*anti*-was exposed to meP-meC.273 for 15 s to 300 s similar to **Figure 3.1**.

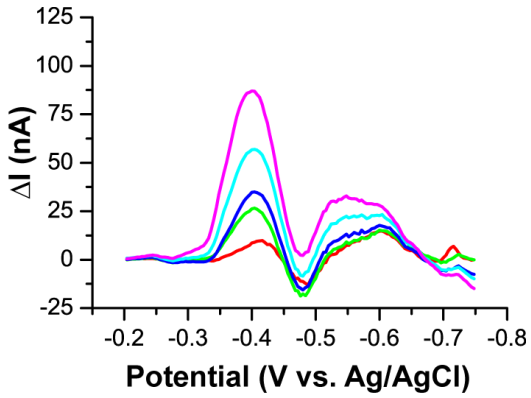

Figure 3.3. Background-subtracted SWV response showing C12-viologen reduction at meP-meC.273 exposed to 100 µM (+)-*anti*-BPDE for 15 s (red), 30 s (green), 60 s (light blue), 180 s (dark blue), and 300 s (pink).

Exposure to (+)-*anti*-BPDE produced higher current responses overall compared to exposure to the racemic solution seen in **Figure 3.1**. This suggests a kinetically faster reaction with the pure enantiomer compared to the racemic solution. Possible reasons for the kinetic rate increase would be the removal of any competing reactions between (+) and (-)-*anti*-BPDE. **Figure 3.4** shows background subtracted SWV plots comparing the standard response when 100 µM (+)-*anti*-BPDE or 200 µM (±)-*anti*-BPDE was exposed to the three different methylated DNA oligomer combinations for 180 s.

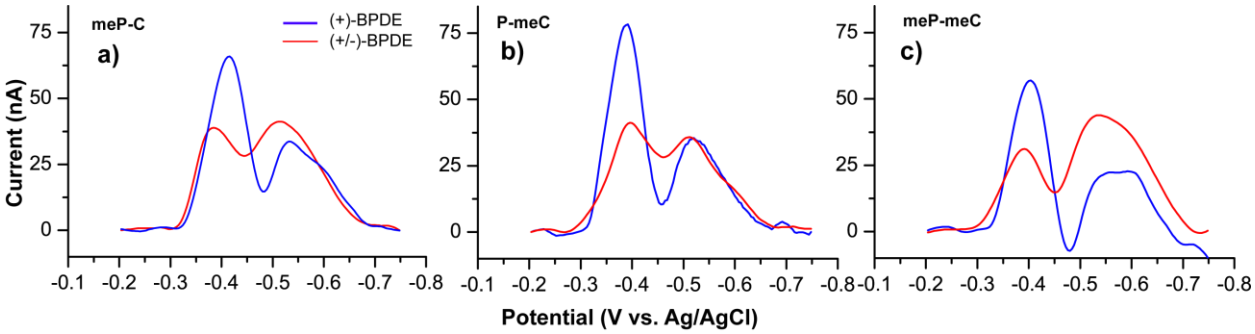

Figure 3.4. Background-subtracted SWV response on A) meP-wtC.273, B) wtP-meC.273, and C) meP-meC.273 modified electrodes due to exposure to (±)-*anti*-BPDE (200 µM, red) or (+)-*anti*-BPDE (100 µM, blue) for 180 s.

Figure 3.4 shows that exposure to (+)-*anti*-BPDE produced much higher current responses at the -0.4 V potential location, and also smaller current response at -0.55 V. However, the overall current response at -0.55 V as a function of total signal was much more significant when using racemic BPDE solutions, which is consistent with reactions of (-)-*anti*-BPDE at DNA locations that force oxidized C12-viologen to adopt a more stable binding arrangement. A plot showing the average peak current ratio (i_p) of the two peaks with the different BPDE solutions on the three oligomeric combinations is shown in **Figure 3.5**. Overall, it is clear that methylation affects BPDE binding to the DNA, which influences the eventual C12-viologen voltammetry.

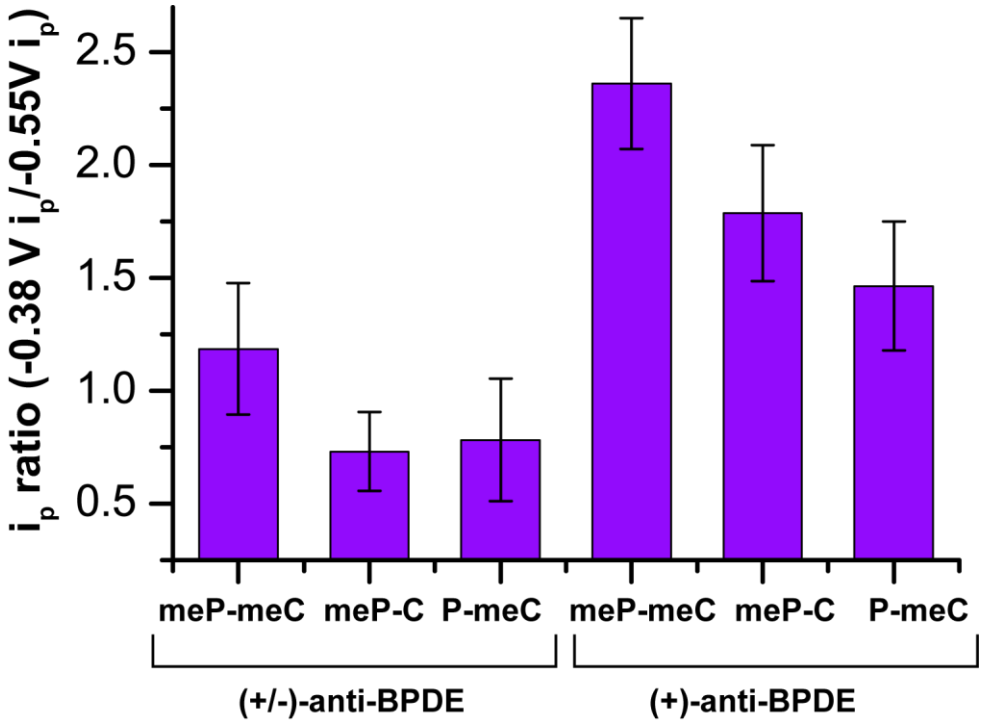

Figure 3.5. i_p ratio (-0.38 V/-0.55 V) comparison for different methylated oligomer combinations (n = 3) exposed to racemic (200 μM) or enantiomerically pure *anti*-BPDE (100 μM) solutions for 300 s.

Discussion

The appearance of multiple C12-viologen peaks as BPDE was exposed to methylated DNA suggests that two main DNA-bound C12-viologen redox active populations change upon BPDE exposure. The reduction is most likely two isolated one-electron reductions of the viologen groups within the molecules, as a two-electron reduction of the viologen would be unlikely. Reduction in this manner from V^{2+} to V^0 (V = viologen) is unlikely because the $V^{+1/0}$ reduction potential is negative shifted (approximately -0.8 V vs. Ag/AgCl) from the $V^{2+/1+}$ potential. Also, the neutral C12-viologen molecule is insoluble and precipitates onto the electrode, which is accompanied by a lack of current response at more negative potentials. [1]

In a previous publication, [4] we postulated that the emergence of the positive shifted SWV -0.4 V peak in BPDE exposed dsDNA was consistent with C12-viologen aggregation external to the DNA helix as depicted in **Figure 3.6**.

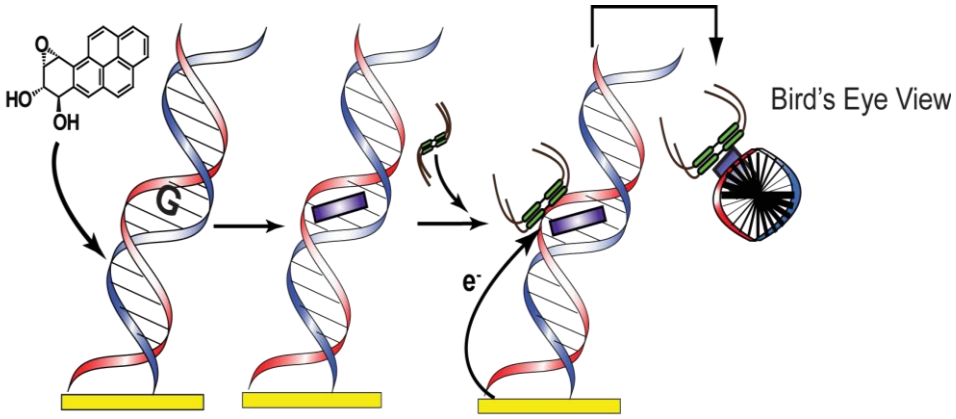

Figure 3.6. Schematic showing (+)-*anti*-BPDE damage to wt.273 oligomers, and the resulting minor groove bound BPDE-guanine adduct. Bird's eye view shows hypothesized aggregation of C12-viologen.

C12-viologen would be expected to aggregate in this manner if a protruding hydrophobic site was formed on the DNA helix upon reaction with *anti*-BPDE. Adduction of the (±)-*anti*-BPDE to guanine would be expected to produce two different positional adducts aligned in opposite directions in the wt.273 minor groove depending on the stereoisomer. (−)-*trans*-*anti*-BP-Gua is known to align toward the 3' side of the adducted DNA strand while the (+)-*trans*-*anti*-BP-Gua aligns towards the 5' side. [6] The current increase at -0.4 V is approximately 70 mV positive of the C12-viologen formal redox potential. This suggests that the viologen in this population is actually destabilized in the oxidized (V^{2+}) form and that the driving force for reduction at that

potential is the formation of face-to-face dimers via overlap of singly occupied π* orbitals.[4] Therefore, the peak growth seen previously using wt.273 damaged with racemic BPDE solutions was ascribed to the C12-viologen bound externally. The significant peak growth at -0.4 V when methylated codon 273 oligomers were exposed to (±)-*anti*-BPDE suggests that minor groove-located BPDE adducts were also formed on these helices.

The emergence of a peak approximately 100 mV negative shifted vs. the C12-viologen formal potential suggests a more stabilized oxidized viologen form (V^{2+}) on the DNA hybrids. In previous work studying C12-viologen voltammetry differences in the presence of ssDNA vs. dsDNA, it was shown that C12-viologen binds to dsDNA in two distinct populations based on the DNA structure.[1] Multiple-populations were not seen on ssDNA presumably because of the lack of a rigid helical structure. The negative shifted redox wave was explained by the stability imparted to C12-viologen by dsDNA and geometric as well as spectroscopic evidence showed that the minor grove was a likely binding site.

The emergence of the negative-shifted SWV peak when BPDE was exposed to methylated DNA suggests the emergence of a C12-viologen population that is stabilized by the DNA structure. Peak growth at this potential was negligible in experiments using non-methylated wt.273.[4] The significant peak growth of the -0.55 V peak here suggests that cytosine methylation within the codon 273 oligomer alters *anti*-BPDE binding in such a way to stabilize C12-viologen binding.

Methylated cytosines located 5' to guanines have been shown to alter the BPDE adduct such that it can orient within the helix differently as opposed BPDE bound on non-methylated sequences. BPDE initially intercalates within the DNA helix before covalent adduction to guanine.[6] The adduction of (±)-*anti*-BPDE to guanine creates a trans-BPDE-guanine adduct.

Following a rearrangement, the *anti*-BPDE adducts predominantly reside in the minor groove after guanine adduction. The methyl group on the 5-C on the cytosine protrudes into the major groove and increases the hydrophobicity of that environment. An *anti*-BPDE adduct that might otherwise orient within the minor groove now experiences added hydrophobic interactions upon intercalation leading to rearrangement and eventual positioning in that intercalated environment. This process is much more prevalent for (−)-*anti*-BPDE adducts as opposed to (+)-*anti*-BPDE adducts, as the (+)-*anti*-BPDE-guanine adduct does not experience the additional hydrophobic interactions based on its steric configuration. [6,7] Therefore, DNA would be expected to exhibit approximately 50% intercalated BPDE adducts and 50% minor groove bound adducts upon exposure to the racemic *anti*-BPDE solution. The intercalation of the BPDE adduct results in guanine base displacement so that the purine face of the guanine aligns within the minor groove.[6] This situation is precisely what the C12-viologen SWV plots in **Figure 3.1** and **Figure 3.4** show. Upon exposure to racemic (±)-*anti*-BPDE, the more positive shifted peak is consistent with C12-viologen oriented external to the helix, as discussed previously, and is due to the minor groove bound BPDE adduct. The negative shifted peak is consistent with C12-viologen bound within the minor groove, in a stabilizing environment. The stabilization arises from possible π system overlapping interactions between the guanine and the viologen. This is shown schematically in **Figure 3.7**.

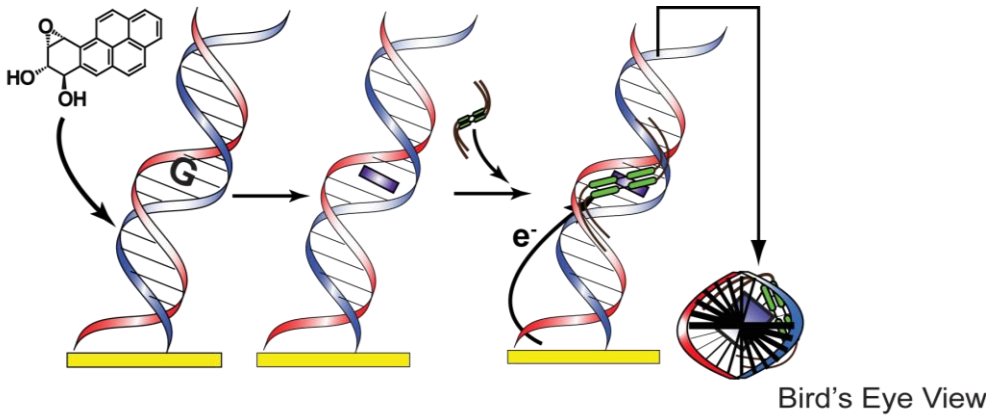

Figure 3.7. Schematic of intercalating BPDE adducts resulting in a stabilizing binding environment for C12-viologen.

Such interactions were shown to have a similar impact on the viologen formal potential, as the electron donating effect of the planar guanine system stabilizes the oxidized viologen. [8] **Figure 3.5** shows that the i_p ratio from the reduction of these two C12-viologen populations is approximately 50-50 when methylated DNA oligomers were exposed to racemic *anti*-BPDE solutions, supporting these claims. Additionally, spectroscopic evidence showed increasing amounts of π–π^* interactions when (±)-*anti*-BPDE was exposed to methylated DNA oligomers, which provides additional support to the increasing amounts of intercalated adducts using these oligomers, leading to the subsequent current increases at the negative shifted potential. [9]

The use of (+)-*anti*-BPDE provided further insight into the current changes at the two potentials. The increasing peak heights are suggestive of a kinetically faster reaction, and (+)-*anti*-BPDE has been shown to be much more active toward damaging guanine as compared to (-)-*anti*-BPDE or *syn*-BPDE. [6,10] The faster kinetics is manifested in higher currents, which is consistent with higher aggregation of C12-viologen outside of the DNA helix. This is expected as (+)-*anti*-BPDE is known to adopt a minor groove location upon binding at guanine sites in

hotspot codons. The aforementioned solution-phase UV spectroscopic experiments using enantiomerically pure (+)-*anti*-BPDE exposed to methylated DNA oligomers were also consistent with this finding. [9]

However, based on the electrochemical signals, (+)-*anti*-BPDE does not exclusively adopt minor groove bound adducts. This is based on the smaller -0.55 V peak increase in the SWV voltammograms using enantiomerically pure BPDE exposed to the different methylated oligomers. The **Figure 3.5** ratio plot also shows that the -0.37 V to -0.55 V i_p ratio is about 2:1 using (+)-*anti*-BPDE. The ratio alters a bit depending on the oligomer employed. The varying amount of intercalated versus minor groove located adducts most likely reflects the differences in sequence contexts that direct the binding of BPDE to the DNA. It has been shown that 5-meC is a primary factor that directs the preferential binding of BPDE to DNA. [7,11] The methylated sequences in the oligomers employed here have either a 5'-^{me}CGT-3' or a 5'-^{me}CGC-3' sequence depending on whether the probe or complement was methylated, or both. The peak current ratio was lowest when the methylated probe strand (meP-wtC.273 sequence) was employed. This is indicative of higher levels of adduct heterogeneity using this sequence. [9] BPDE adducts have been shown to be highly dependent on the third base in the sequence, which dictates the rigidity of the eventual BPDE adduct. CGC and CGT sequences have been shown to be much more rigid and less easily repaired in vivo, while those in TGT sequences are more fluid and are more easily repaired. [7,12]

Conclusions

This study significantly expanded the findings of work previously done in our lab to electrochemically detect sequence specific DNA damage. Here, a key epigenetic factor, cytosine methylation was studied, and the electrochemical response was significantly different than what was seen when using wild type DNA, or DNA with no methylation. The electrochemical response upon BPDE damage showed increases at two potentials based on how C12-viologen bound to the damaged DNA. Cytosine methylation fundamentally alters how BPDE binds to DNA, and these subtle changes are detectable in the sensor based on how they influence the binding our C12-viologen to the complex.

Secondly, these electrochemical findings were further supported by using epigenetically pure (+)-*anti*-BPDE, which produced much larger peak growth at -0.38 V upon exposure to DNA oligomers. (+)-*anti*-BPDE is known to predominately adopt minor groove bound adducts, and the large current increases at that potential are consistent with that expectation. Overall, this sensor has the ability to not only detect sequence specific DNA damage, but also report on the morphology of the resulting adduct, providing a significant amount of information when studying genotoxic processes at key DNA sequences.

References

1. Hvastkovs, E. G.; Buttry, D. A. Minor Groove Binding of a Novel Tetracationic Diviologen. *Langmuir* **2006**, *22*, 10821-10829.

2. Hvastkovs, E. G.; Buttry, D. A. Characterization of Mismatched DNA Hybridization via a Redox-Active Diviologen Bound in the PNA−DNA Minor Groove. *Langmuir* **2009**, *25*, 3839-3844.

3. Satterwhite, J. E. Electrochemical Detection of Benzo[*a*]pyrene Metabolite DNA Damage: Implications of Nucleobase Sequence and Adduct Stereochemistry. M.S. Thesis, East Carolina University, Greenville, NC, 2011.

4. Satterwhite, J. E.; Pugh, A. M.; Danell, A. S.; Hvastkovs, E. G. Electrochemical Detection of *anti*-Benzo[*a*]pyrene Diol Epoxide DNA Damage on *TP53* Codon 273 Oligomers. *Anal. Chem.* **2011**, *83*, 3327-3335.

5. Zhang, N.; Lin, C.; Huang, X.; Kolbanovskiy, A.; Hingerty, B.; Amin, S.; Broyde, S.; Geacintov, N. E.; Patel, D. J. Methylation of Cytosine at C5 in a CpG Sequence Context Causes a Conformational Switch of a Benzo[*a*]pyrene diol epoxide-N^2-guanine Adduct in DNA from a Minor Groove Alignment to Interacalation with Base Displacement. *J. Mol. Biol.* **2005**, *346*, 951-965.

6. Geacintov, N. E.; Cosman, M.; Hingerty, B. E.; Amin, S.; Broyde, S.; Patel, D. J. NMR Solution Structures of Stereoisomeric Covalent Polycyclic Aromatic Carcinogen– DNA Adducts: Principles, Patterns, and Diversity. *Chem. Res. Toxicol.* **1997**, *10*, 111-146.

7. Pradhan, P.; Gräslund, A.; Seidel, A.; Jernström, B. Implications of Cytosine Methylation on (+)-*anti*-Benzo[*a*]pyrene 7,8-Dihydrodiol 9,10-Epoxide N^2-dG Adduct Formation in 5'-d(CGT), 5'-d(CGA), and 5'-d(CGC) Sequence Contexts of Single- and Double- Stranded Oligonucleotides. *Chem. Res. Toxicol.* **1999**, *12*, 816-821.

8. Balzani, V.; Bandmann, H.; Ceroni, P.; Giansante, C.; Hahn, U.; Klärner, F.; Müller, U.; Müller, W. M.; Verhaelen, C.; Vicinelli, V.; Vögtle, F. Host-Guest Complexes between an Aromatic Molecular Tweezer and Symmetric and Unsymmetric Dendrimers with a 4-4'-Bipyridinium Core. *J. Am. Chem. Soc.* **2006**, *128*, 637-648.

9. Satterwhite, J. E.; Trumbo, C. M.; Danell, A. S.; Hvastkovs, E. G. Electrochemical Study on the Effects of Epigenetic Cytosine Methylatoin on *Anti*-Benzo[*a*]pyrene Diol Epoxide Damage at TP53 Oligomers. *Anal. Chem.* **2013**, *85*, 1183-1191.

10. Chen, F. M. Denaturation and Renaturation Studies of Benzo[*a*]pyrene Metabolite Modified DNAs. *Biochemistry* **1987**, *26*, 4323-4331.

11. Glick, J.; Xiong, W.; Lin, Y.; Noronha, A. M.; Wilds, C. J.; Vouros, P. The influence of cytosine methylation on the chemoselectivity of benzo[a]pyrene diol epoxide-oligonucleotide adducts determined using nanoLC/MS/MS. *J. Mass. Spectrom.* **2009**, *44*, 1241-1248.

12. Cai, Y.; Patel, D. J.; Geacintov, N. E.; Broyde, S. Dynamics of a Benzo[a]pyrene-derived Guanine DNA Lesion in TGT and CGC Sequence Contexts: Enhanced Mobility in TGT Explains Conformational Heterogeneity, Flexible Bending, and Greater Susceptibility to Nucleotide Excision Repair. *J. Mol. Biol.* **2007**, *374*, 292-305.

CHAPTER 4: DETECTION OF DNA DAMAGE FROM BIOACTIVATED BENZO[*A*]PYRENE

Results

Previous results suggested that the oligomeric DNA damage sensor is useful in detecting sequence specific damage as well as the orientation of the adduct within the oligomer. However, previous work was all performed with direct damaging agents. To study the bioactivation process, enzymatic models as well as bio-relevant enzymes needed to be incorporated into the sensor. Ideally, this would involve the incorporation of cytochrome (cyt) 450s, which are heavily involved in the first stages of metabolism involving oxidation of xenobiotics. The use of human cyt P450 enzymes will allow for more accurate toxicity predictions as well as help determine which cyt P450 isoforms are involved in BP bioactivation. Cyt P450 enzymes are heme-containing metabolic enzymes that perform many functions, but catalyze the oxidation of organic substances through the transfer of oxygen atoms. The enzymatic cycle that these enzymes employ in vivo is shown in **Figure 4.1**. The figure shows that there are numerous avenues in the bioactivation, or substrate oxidation process. In vivo, cyt P450 undergoes two-electron reduction via its redox partner, cytochrome P450 reductase (CPR), and incorporation of molecular oxygen to enter into the iron(IV)oxo cation radical state. This is the active form of the heme center that oxidizes the substrate. Alternatively, the cycle can be shunted via the introduction of hydrogen peroxide to force the heme to immediately enter into into the iron-peroxo state that can then become the cation radical. This shunt is biorelevant in cases of oxidative stress, where reactive oxygen species can overwhelm the cell. [1]

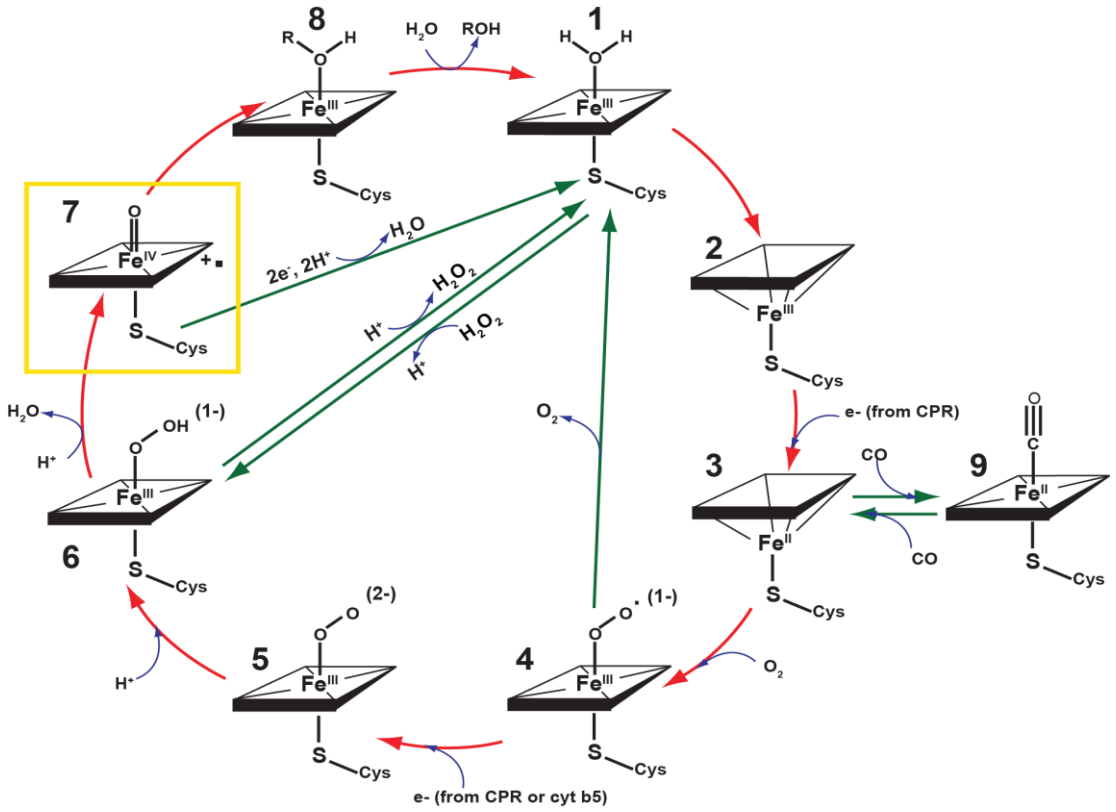

Figure 4.1. The heme enzymatic cycle involved in cytochrome P450 metabolism.

Cyt P450 enzymes are responsible for BP bioactivation. Specifically, it has been shown that the cyt 1 family (1A1 and 1B1) are responsible for the majority of BP metabolism.[2, 3] The reactive BP metabolites that are produced can form adducts with DNA. However, the use of cytochrome P450s in sensor work is complicated by the tedious work needed to purify or expense associated with their acquisition. One way to provide a degree of biological activity that mimics cyt P450 action is to use myoglobin (Mb) as a heme enzyme mimic. Mb is inexpensive and can be obtained in gram amounts. While not typically known as a bioactivation enzyme, it can be activated and can act like a cyt P450 by using H_2O_2 to shunt the metabolic cycle. Using

H_2O_2 in small concentrations has been used to activate Mb and other cyt P450s in sensors involving genotoxic xenobiotics, including BP. One drawback is that hydrogen peroxide can damage DNA itself, but at lower concentrations, it has been shown to not significantly influence DNA damage signals acquired electrochemically. [2]

An idealized scheme utilizing enzymes in the DNA damage sensor is shown in **Figure 4.2**. The figure shows how BP is metabolized into a variety of reactive molecules by cyt P450, epoxide hydrolase (EH), or myoglobin. The reactive metabolites can bind to DNA, which then changes the interaction of C12-Viologen with the helix, providing similar electrochemical responses as seen and described in Chapter 3.

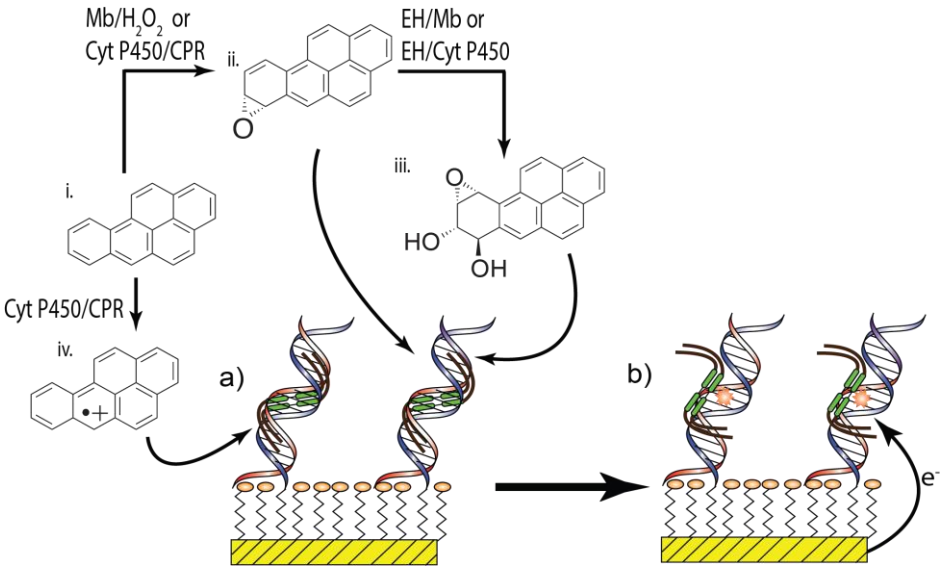

Figure 4.2. An idealized scheme showing how bioactivation enzymes can be incorporated into the DNA damage sensor.

Gold electrodes were modified as discussed in previous chapters, using the wt.273 21-mer oligomer DNA sequence spanning codons 270-276 of the TP53 gene. The initial plan of attack to incorporate Mb was to expose DNA-modified electrodes to a *solution-phase* reaction mixture containing varying concentrations of BP, 250 nM H_2O_2 and 3 mg/mL myoglobin for increasing times from 15 to 600 sec. **Figure 4.3** shows the background SWV responses obtained when 100 μM BP was used in the enzyme solution exposed to wt.273. The figure shows that significant peak growth was seen at both -0.50 V and -0.37 V, which was previously shown to be due to intercalating and minor groove located BP adducts, respectively.

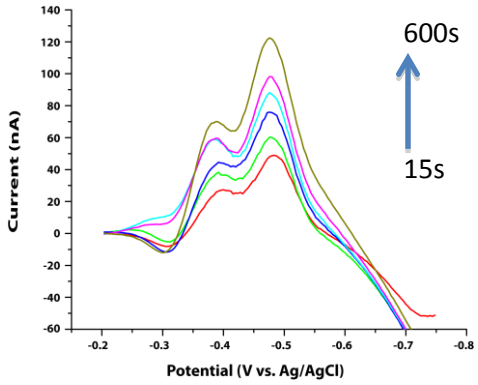

Figure 4.3. Background-subtracted SWV response showing C12-viologen reduction as wt.273 was exposed to a solution phase Mb-BP damage solution containing 100 μM BP, 250 nM H_2O_2 and 3 mg/mL Mb for 15 s (red), 30 s (green), 60 s (dark blue), 180 s (light blue), 300 s (pink), and 600 s (dark yellow).

These initial responses were promising, but control experiments designed to show that the signals obtained were due to DNA damage showed otherwise. **Figure 4.4** shows these SWV responses from control experiments involving electrode exposure to the various combinations of the BP/H_2O_2/Mb solution. Muted signals were the expected result for these controls when any

component of the solution was missing. This was especially true when the reaction mixture was missing BP as no BP-DNA adducts could form. Additionally, when the reaction mixture was missing H_2O_2, Mb should not have been activated, which would result in no bioactivation of BP and no way for BP to form covalent DNA adducts.

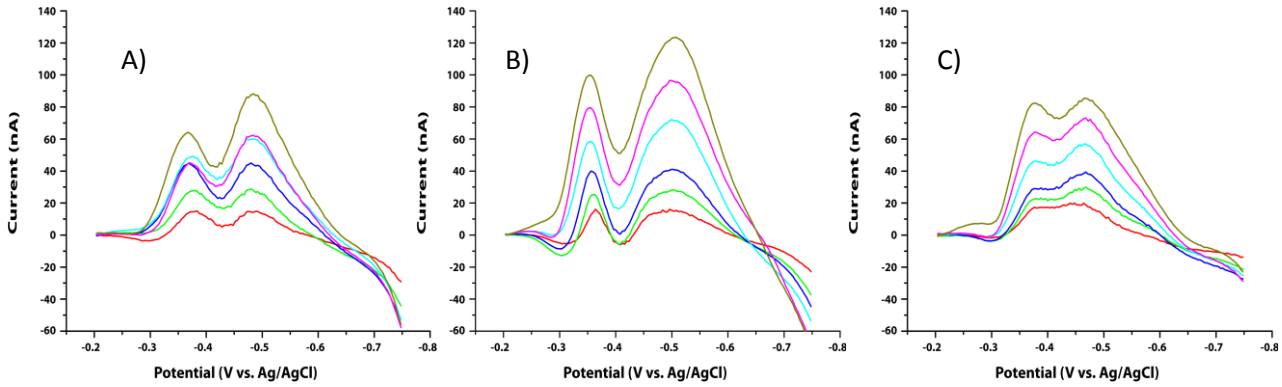

Figure 4.4 Background-subtracted SWV response showing C12-viologen reduction as wt.273 was exposed to solution phase Mb-BP damage solutions for 15 s (red), 30 s (green), 60 s (dark blue), 180 s (light blue), 300 s (pink), and 600 s (dark yellow). A) Mb + H_2O_2. B) Mb + 100 μM BP. C) 3mg mL^{-1} Mb only.

Large responses at both key potentials were seen in all control plots. **Figure 4.4C** shows that these large responses are seen only when Mb was exposed to the electrode surface – i.e. no BP or H_2O_2. This shows that Mb can bind non-specifically on the electrode surface and C12-viologen then associates within the Mb/DNA electrode in some way. While some BP bioactivation might be occurring leading to DNA damage, non-specific binding of Mb presumably provided additional aggregation sites for the C12-viologen, producing large currents at the two key potentials. This is shown schematically in **Figure 4.5**. This non-specific binding obviously produces interfering currents, which meant that additional steps or an alternative method to study the bioactivation process was necessary.

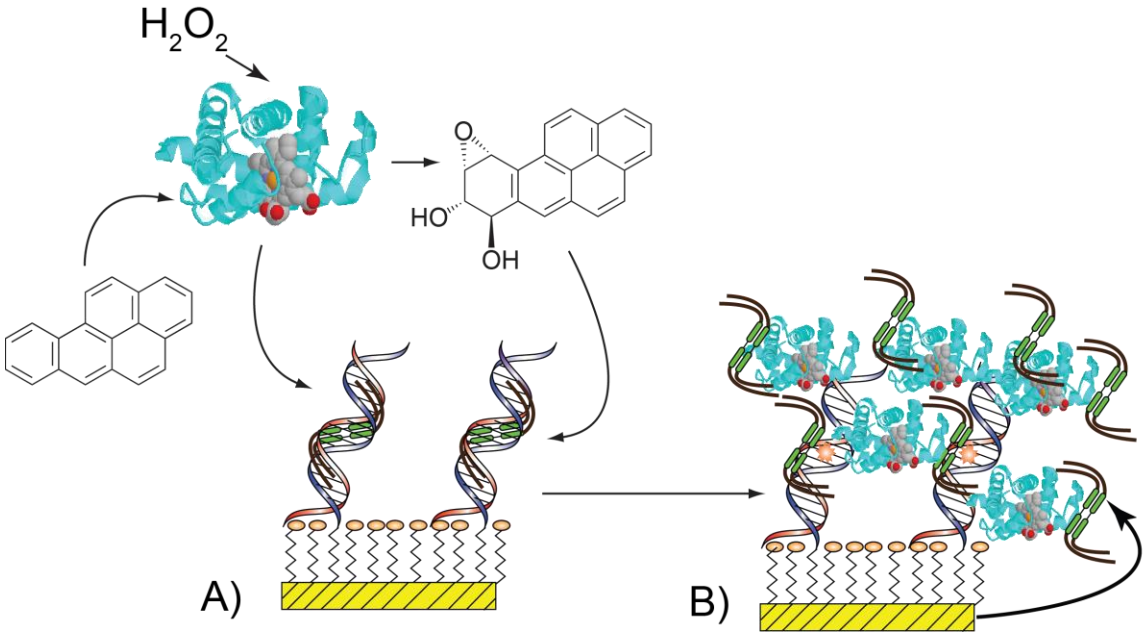

Figure 4.5. A) dsDNA modified electrode exposed to Mb, H_2O_2, and BP reaction in solution. B) Non-specific binding of Mb leading to C12-viologen aggregation, which interferes with the SWV output.

Several approaches were employed to try and counteract non-specific binding. First, an electrode was exposed to only Mb followed by a rinse after each time point with a buffer of pH 8.0 to remove excess Mb**.** The isoelectronic point of Mb is approximately 6.5; [4] therefore, it was hypothesized that a basic pH would cause electrostatic repulsion of the Mb from the anionic DNA surface. Additionally, a rinse after each time point with a pH 8.0 buffer containing 0.05% polyethylene glycol (PEG solution) was used by soaking the electrode in Mb for 5 minutes, running a SWV, then rinsing in PEG solution for 5 minutes, then obtaining a second SWV. In either case, the signals did not decrease after rinsing which shows the buffer rinsing steps were not effective in removing excess Mb that contributed to the current changes.

The final avenue explored to incorporate Mb into the sensor was to allow Mb to saturate the electrode surface before exposure to buffer solutions containing BP and H_2O_2. We speculated that C12-viologen would bind to both Mb and DNA, but that this pre-saturation step would allow for changes to the DNA to be more easily monitored. This is depicted schematically in **Figure 4.6**.

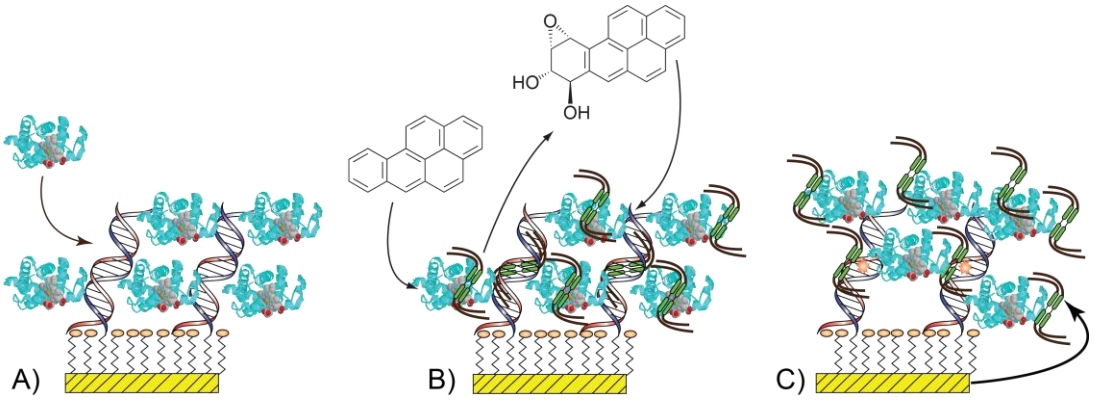

Figure 4.6. Scheme showing the pre-saturation of Mb before DNA damage. A) Shows the adsorption of Mb over exposure time, which can be monitored via SWV reduction of C12-viologen. The saturated electrode (B) can then be exposed to BP and H_2O_2 to activate the Mb. DNA damage can then be monitored via changes in the SWV plots using the pre-saturated Mb signal as the background.

Raw data shown in **Figure 4.7A** shows SWV plots before adding Mb (black), followed by pre-adsorption of Mb onto the electrode allowing saturation of the electrode surface before exposure to BP and H_2O_2. Mb adsorption was monitored in a timed fashion, removing the electrode from the Mb at various time intervals before monitoring using SWV in the presence of C12-viologen. When the C12-viologen current increase plateaued as seen in an unchanging SWV plot from one Mb exposure to the next, it was assumed that Mb had saturated the electrode

surface. This typically took 30 min of Mb exposure to reach this point. The last acquired SWV was then the t = 0 s plot that would be subtracted from subsequent BP/H_2O_2 exposure runs.

Figure 4.7B shows the raw data C12-viologen reduction SWV plots at a wt.273 modified electrode after pre-adsorption of Mb and then exposed to 100 µM BP and 250 nM H_2O_2. **Figure 4.7C** shows the resulting background subtracted SWV plots by subtracting the blue SWV in **Figure 4.7A** from the SWV in **Figure 4.7B**. The plots clearly show significant current increase at approximately -0.37 V with very little current increase at -0.50 V.

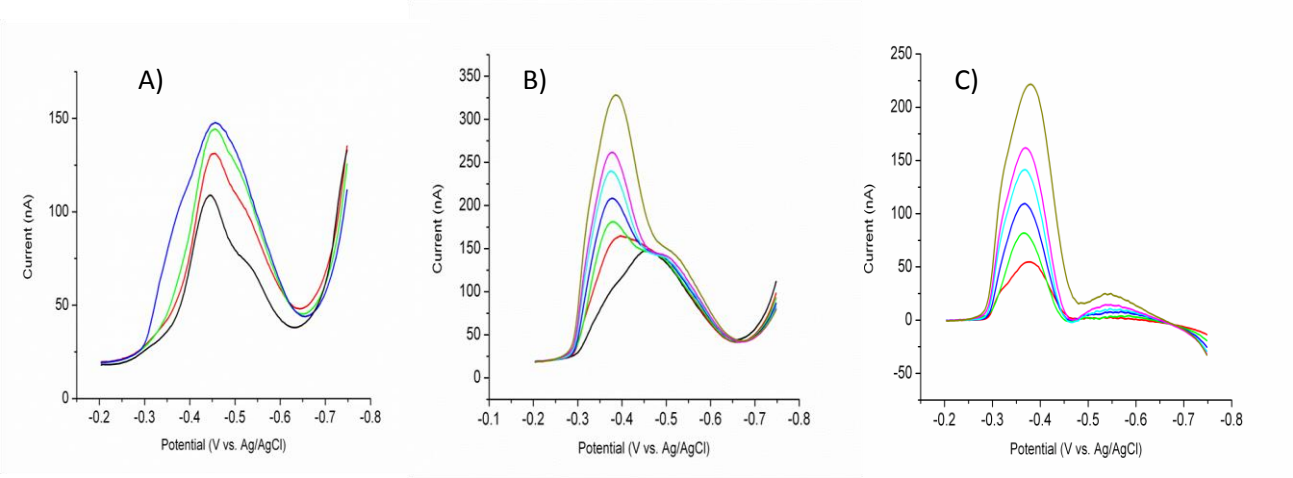

Figure 4.7. A) Raw SWV response showing saturation of Mb on the electrode surface. The plots represent monitoring over 30 min. B) Raw SWV response showing C12-viologen reduction on the electrode upon addition of 100 µM BP and 250 nM H_2O_2 after pre-adsorption of Mb for 15 s (red), 30 s (green), 60 s (dark blue), 180 s (light blue), 300 s (pink), and 600 s (dark yellow). C) Resulting background subtracted SWV plot. Plots in B) subtracted from blue plot in A).

Figure 4.8 shows different combinations at 5 min exposure to 100 µM BP and 250 nM H_2O_2 including controls. All runs were first saturated with Mb before exposure to the reaction

mixture. The plots show that the C12-viologen reduction current that emerges after xenobiotic exposure is dramatically muted in situations where BP and H_2O_2 are not exposed together as well as in situations where a control DNA sequence is used where the codon 273 guanine was replaced with a cytosine. Controls using ethylenediaminetetraacetic acid (EDTA) and butylated hydroxyanisole (BHA) were employed to show that hydroxyl radicals were not the source of the current increase. The significance of these controls is discussed further below.

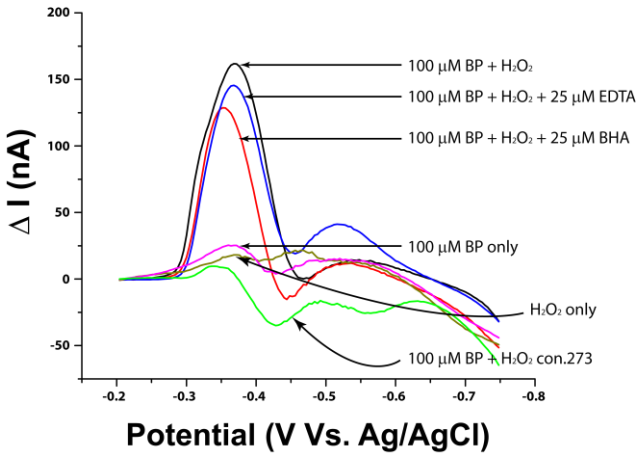

Figure 4.8. Background-subtracted SWV response at 5 min showing C12-viologen reduction as wt.273 was exposed to 100 µM BP + 250 nM H_2O_2 (black), 100 µM BP + H_2O_2 + 25 µM EDTA (blue), 100 µM BP + H_2O_2 + 25 µM BHA (red), 100 µM BP only (pink), H_2O_2 only (dark yellow) or con.273 exposed to 100 µM BP + H_2O_2 (green).

Electrochemical peak current response at -0.37 V was found to be dependent on BP concentration. This is shown in **Figure 4.9A**. At 1 min BP exposure, the -0.37 V peak height increases with BP concentration from 10 µM to 100 µM.

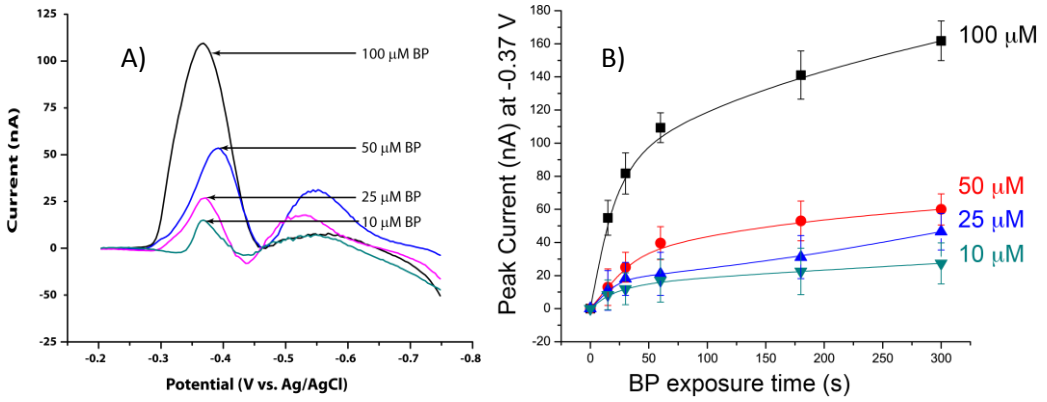

Figure 4.9. A) Background subtracted SWV plots showing the response at 60 s BP + H_2O_2 exposure for different concentrations of BP. B) Peak current at -0.37 V vs. BP exposure time plots for the different concentrations of BP.

Figure 4.9B shows the peak current vs. time responses for the different concentrations of BP exposed to the Mb/DNA-modified electrodes. The increase in reaction rate as the BP concentration is increased was expected. The initial slopes of the plots in Figure 5.9B allow for the assessment of apparent first order enzyme kinetics information. Additional cyclic voltammetry (CV) experiments were conducted in order to assay and quantify the amount of Mb present on the electrode surface. Through the integration of the reduction peak at approximately -0.3 V vs. Ag/AgCl on these electrodes, it was found that approximately 21 (±2) pmol Mb cm^{-2} adsorbs on the electrode surface. This allowed a relative turnover calculation for Mb of 1.82 (±0.50) min^{-1} pmol Mb^{-1}. Compared to previous reports studying BP activation and subsequent DNA damage by Mb in layer-by-layer (LbL) films, [2] this is actually a much higher turnover value. This may reflect the ultimate sensitivity of the detection approach employed here.

Discussion

Overall, the incorporation of enzymes into the DNA damage sensor was a lesson in learning from numerous failures. Initial studies designed to monitor DNA damage using solution phase enzymatic reactions were promising. However, the controls designed to prove that DNA damage was being monitored showed that Mb significantly adsorbs to the electrode surface. Beyond the adsorption of Mb; however, was the fact that C12-viologen also aggregates onto the Mb that adsorbs on the electrode surface, which further convoluted signals that were obtained. Several avenues were explored to counteract the adsorption of Mb. Several different buffer and surfactant solution washes were employed, but these rinses did little to remove the Mb signal.

Real progress in detecting DNA damage came from changing the approach taken to incorporate the Mb into the sensor. Instead of performing solution phase reactions, the Mb was allowed to adsorb onto the DNA surface. In this fashion, the electrode was modified using a hybrid LbL technique where the DNA hybridization electrode was modified with a layer of Mb. In this manner, the electrode is more intricate than a standard LbL DNA damage electrode as we can monitor adduct orientation in addition to relative enzyme kinetics.

Mb was allowed to adsorb onto the surface until the C12-viologen signal saturated. This was monitored by periodically taking the electrode out of the Mb solution and interrogating the electrode in a solution of C12-viologen. By taking the saturated Mb SWV as t = 0s background, this allowed the elucidation of changes to the electrode surface due to DNA damage. This is evident from the control plots seen in **Figure 4.8**. First, the control using the modified DNA sequence where cytosine was substituted for guanine in the wt.273 sequence shows that the signal changes that are detected are indeed due to DNA damage. The complete removal of signal change when this site in the DNA was removed is clear evidence that we are monitoring

DNA damage at that particular guanine. This was previously shown to be the case in preliminary work designing the DNA damage sensor.[5] The 273-codon guanine is a known hotspot that is often damaged by BP metabolites and is often mutated in lung cancers.[6-8]

Second, BHA and EDTA controls show that it is reactive BP forms that are damaging the DNA. BHA is known to react with free radicals, including hydroxyl radicals. If hydroxyl radicals were present and contributing to DNA damage, inclusion of BHA would provide a significantly muted response as these hydroxyls would be eliminated. EDTA is a chelating agent responsible for sequestering certain metal ions, including $Fe^{2/3+}$. Hydroxyl radicals can be produced when metal complexes react with H_2O_2 in a process known as the Fenton reaction. Therefore, inclusion of EDTA would sequester any iron impurities if they were present, resulting in lower electrochemical signals as no hydroxyl radicals could form. Both BHA and EDTA controls show little differences in reduction in current suggesting that the large peak currents at -0.37 V from BP-H_2O_2 exposure were due to BP metabolites adducting to the guanine hotspot site within the DNA.[9]

The DNA damage sensor was shown to exhibit much faster relative Mb turnover compared to previous studies employing Mb to activate BP.[2] This might be related to the DNA employed in this study vs. the larger calf thymus DNA and electrochemical detection approach utilized in the earlier study. The C12-viologen assay here is a derivative method, and as such has the ability to provide relatively high S/N as the background signal is removed leaving behind only signal due to DNA damage. Also, the use of gold electrodes here provided less Mb than the LbL approach used previously. All of these aspects likely lead to the higher sensitivity of the approach described here.

An interesting finding in the detection of bioactivated DNA damage is that the majority of the signal detected was at the -0.37 V potential. In Ch. 2, it was shown that the C12-viologen reduction signal can be modulated based on DNA methylation and the subsequent BP adduction site. The large peak at -0.37 V suggests that the reactive BP metabolite that is formed from Mb metabolism is a minor groove bound species. Minor groove bound BP adducts force aggregation of the C12-viologen external to the DNA helix and give rise to reduction at potentials positive of the formal potential (E^f). [5]

Minor groove bound DNA adducts have been shown to be much more carcinogenic compared to the intercalated counterparts. The highly carcinogenic (+)-anti-BPDE metabolite, for instance, almost exclusively forms minor groove bound adducts when it adducts guanine. [10-13] Methylated DNA was not employed in this study, so further electrochemical analysis of the adduct type is not possible, but it is clear that a reactive metabolite that has the ability to align in the DNA minor groove was produced by Mb. The ability of the sensor to detect reactive metabolite DNA damage is promising for future studies involving biologically relevant cyt P450s. Since different cyt enzymes show different affinity toward BP and some such as cyt P450 1A1 and 1B1 have been shown to be highly efficient in the bioactivation of BP, [2] the sensor here should be able to discern not only the relative enzyme kinetics of different P450 isoforms, but also detect which isoforms lead to more dangerous minor groove bound adducts.

References

1. Rusling, J. F.; Hvastkovs, E. G.; Schenkman, J. B. Toxicity screening using biosensors that measure DNA damage. *Curr. Op. Drug Disc. Devel.* **2007**, *10*, 67-73.

2. Hvastkovs, E. G.; So, M.; Krishnan, S.; Bajrami, B.; Tarun, M.; Jansson, I.; Schenkman, J. B.; Rusling, J. F. Electrochemiluminescent Arrays for Cytochrome P450-Activated Genotoxicity Screening. DNA Damage from Benzo[a]pyrene Metabolites. *Anal. Chem.* **2007**, *79*, 1897-1906.

3. Shimada, T.; Wunsch, R. M.; Hanna, I. H.; Sutter, T. R.; Guengerich, F. P.; Gillam, E. M. J. Recombinant human cytochrome P450 1B1 expression in Escherichia coli. *Arch. Biochem. Biophys.* **1998**, *357*, 111-120.

4. Lvov, Y. M.; Lu, Z.; Schenkman, J. B.; Zu, X.; Rusling, J. F. Direct Electrochemistry of Myoglobin and Cytochrome p450cam in Alternate Polyion Layer-by-Layer Films with DNA and Poly(styrenesulfonate). *J. Am. Chem. Soc.* **1998**, *120*, 4073-4080.

5. Satterwhite, J. E.; Pugh, A. M.; Danell, A. S.; Hvastkovs, E. G. Electrochemical Detection of anti-Benzo[a]pyrene Diol Epoxide DNA Damage on TP53 Codon 273 Oligomers. *Anal. Chem.* **2011**, *83*, 3327-3335.

6. Denissenko, M. F.; Pao, A.; Tang, M.; Pfeifer, G. P. Preferential formation of benzo[a]pyrene adducts at lung cancer mutational hotspots in P53. *Science* **1996**, *274*, 430-432.

7. Denissenko, M. F.; Chen, J. X.; Tang, M.; Pfeifer, G. P. Cytosine methylation determines hot spots of DNA damage in the human P53 gene. *Proc. Nat. Acad. Sci. U.S.A.* **1997**, *94*, 3893-3898.

8. Pfeifer, G. P.; Holmquist, G. P. Mutagenesis in the P53 gene. *Biochimica et Biophysica Acta, Reviews on Cancer* **1997**, *1333*, M1-M8.

9. Satterwhite, J. E. Electrochemical Detection of Benzo[a]pyrene Metabolite DNA Damage: Implications of Nucleobase Sequence and Adduct Stereochemistry , East Carolina University, East Carolina University, 2011.

10. Zhang, N.; Lin, C.; Huang, X.; Kolbanovskiy, A.; Hingerty, B. E.; Amin, S.; Broyde, S.; Geacintov, N. E.; Patel, D. J. Methylation of Cytosine at C5 in a CpG Sequence Context Causes a Conformational Switch of a Benzo[a]pyrene diol epoxide-N2-guanine Adduct in DNA from a Minor Groove Alignment to Intercalation with Base Displacement. *J. Mol. Biol.* **2005**, *346*, 951-965.

11. Yan, S.; Shapiro, R.; Geacintov, N. E.; Broyde, S. Stereochemical, Structural, and Thermodynamic Origins of Stability Differences between Stereoisomeric Benzo[a]pyrene

Diol Epoxide Deoxyadenosine Adducts in a DNA Mutational Hot Spot Sequence. *J. Am. Chem. Soc.* **2001**, *123*, 7054-7066.

12. Pradhan, P.; Graeslund, A.; Seidel, A.; Jernstroem, B. Implications of Cytosine Methylation on (+)-anti-Benzo[a]pyrene 7,8-Dihydrodiol 9,10-Epoxide N2-dG Adduct Formation in 5'-d(CGT), 5'-d(CGA), and 5'-d(CGC) Sequence Contexts of Single- and Double-Stranded Oligonucleotides. *Chem. Res. Toxicol.* **1999**, *12*, 816-821.

13. Broyde, S.; Wang, L.; Zhang, L.; Rechkoblit, O.; Geacintov, N. E.; Patel, D. J. DNA Adduct Structure-Function Relationships: Comparing Solution with Polymerase Structures. *Chem. Res. Toxicol.* **2008**, *21*, 45-52.

CHAPTER 5: FUTURE DIRECTIONS AND CONCLUSIONS

Future Directions

Findings from this project are going to influence future work in two main areas. The first area is the use of mass spectrometry to identify the reactive metabolites and DNA adducts that are produced from Mb metabolism of BP. While our sensor suggests that DNA damage is certainly occurring on the electrode, which was confirmed through several control studies, we still need to validate our sensor response. Initial work in this area has centered around immobilizing wt.273 DNA oligomers and Mb on silica microspheres to generate the conditions necessary for efficient reaction kinetics. The general plan of attack is shown in **Figure 5.1**. Surface immobilization provides the means to increase the concentrations of DNA and enzymes so that the DNA damage reactions can take place in an analytically suitable time frame. DNA on the microspheres can later be collected, adducts hydrolyzed from the DNA chain, and identified via LC-MS methodology. [1]

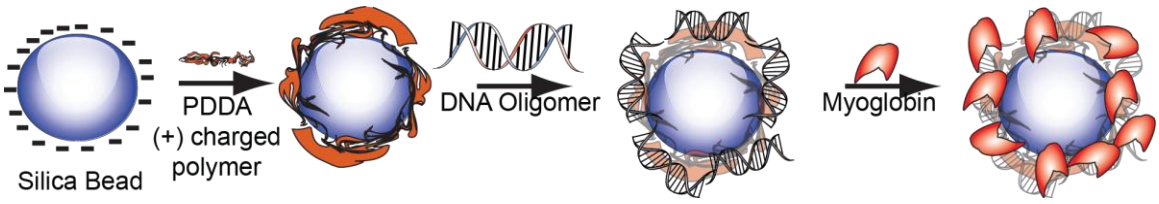

Figure 5.1. Schematic showing steps involved in modifying silica microspheres in a LbL format.

Second, while myoglobin provides a good model, it certainly is not a biologically relevant enzyme in a metabolism sense. To this end, we have several cyt P450 isoforms in bicistronic (reductase + cyt P450 together) membrane fractions that can be immobilized on the electrode in a similar fashion.[1] Membrane fractions exhibit a bit more complexity; however, in that they consist of a lipid membrane containing the enzymes of interest along with several others. Initial studies shown in **Figure 5.2**, however, suggest that it will be possible to study the DNA damage from different P450 isoforms. The figure shows the results of a timed study using cyt P450 1A1 on the left, and the comparisons with cyt P450 1A2 along with relevant controls on the right. Significant peak growth is seen in situations where NADPH + BP are used. NADPH is used to activate the cyt P450 reductase, which in turn can reduce the cyt P450 as shown in Chapter 4 (**Figure 4.1**). BP or NADPH only produces negative peak growth, which we previously postulated to be due to classical intercalation of BP that elongates the oligomer, resulting in lower amounts of electrostatically bound C12-viologen.[2] NAPDH alone did not cause significant peak growth at the studied concentration.

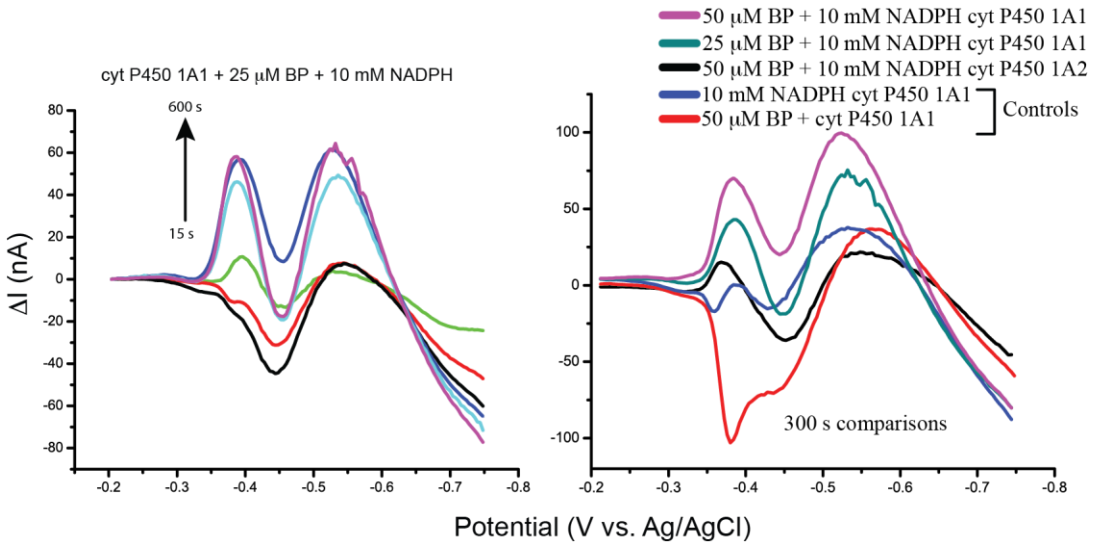

Figure 5.2. Background subtracted SWV showing C12-viologen response at DNA-cyt P450 modified electrodes. Left shows the time response as 25 μM BPDE + 10 mM NADPH was exposed to a cyt P450 1A1 membrane fraction modified electrode. Right shows the comparisons between controls, cyt P450 1A1, and cyt P450 1A2 modifications.

The figure demonstrates that the metabolism of BP produces two main peaks upon C12-viologen reduction, which suggests that the BP was metabolized by the P450 to produce reactive BP metabolites that can either result in minor groove bound or base displacing intercalated DNA adducts. Cyt P450 1A1 was more active toward BP metabolism compared to cyt P450 1A2 over the same time frame. In actuality, the activity of cyt P450 1A1 is much higher than cyt P450 1A2 as the concentration of P450 1A1 is a factor of 10 lower than 1A2 within the membrane fractions. Overall, the significantly higher activity of 1A1 was expected based as cyt P450 1A1 is an inducible form of P450 within the lung, whereas P450 1A2 is primarily expressed within the liver.[3] The introduction of BP into the lung via smoking, for instance, causes cyt P450 to be induced so that BP can be metabolized.

Conclusions

Overall, an electrochemical sensor was constructed that had the ability to not only detect DNA damage, but also provide information on the stereochemistry and location of the DNA adduct within the oligomeric sequence. The use of methylated cytosines at the 5' position to the hotspot guanine in the DNA sequence drastically altered the electrochemical signal obtained when C12-viologen was reduced on the DNA-modified electrode. Previously, we showed that the primary location of current growth was at a potential of -0.37 V vs. Ag/AgCl, which was positive of the E^f of C12-viologen.[2] This suggested aggregation of C12-Viologen at external helix locations, consistent with a minor groove BPDE adduct within the DNA oligomer. When methylated cytosines were present, we showed that two locations of current growth were seen. In addition to the -0.37 V peak, we also saw a peak negative shifted from the E^f at -0.55 V. The growth at the negative shifted potential was consistent with C12-viologen bound within the minor groove of the DNA, which was further consistent with an base-displacing intercalated BPDE adduct. These adducts were based on the stereochemistry of the BPDE, and showed that our sensor has the ability to glean a large amount of biologically important information in a relatively rapid and inexpensive manner.

In addition to the information obtained using methylated cytosine-modified DNA, we also showed that the sensor has the ability to detect gene-specific DNA damage from bioactivated metabolites. To subvert adsorption issues that plagued our initial studies, electrodes were modified with DNA hybrids and layered with Mb, forming a pseudo-LbL electrode. Using the heme model, myoglobin, we showed that electrochemical signals were obtained that are consistent with DNA damage at the hotspot guanine. The sensor produced signals that exhibited enhanced enzyme kinetics compared to previous LbL studies, which may

have been due to the use of short oligomeric sequences. Further, the primary peak growth at -0.37 V suggested that Mb produces reactive BP metabolites that can bind in the minor groove of DNA. Minor groove-bound adducts have been shown to be much more carcinogenic in vivo. These initial studies provided the key steps into furthering this project with biologically important cyt-P450 enzymes in the future.

References

1. Hvastkovs, E. G.; Schenkman, J. B.; Rusling, J. F. Metabolic Toxicity Screening Using Electrochemiluminescence Arrays Coupled with Enzyme-DNA Biocolloid Reactors and Liquid Chromatography–Mass Spectrometry. *Ann. Rev. Anal. Chem.* **2012**, *5*, 79-105.

2. Satterwhite, J. E.; Pugh, A. M.; Danell, A. S.; Hvastkovs, E. G. Electrochemical Detection of anti-Benzo[a]pyrene Diol Epoxide DNA Damage on TP53 Codon 273 Oligomers. *Anal. Chem.* **2011**, *83*, 3327-3335.

3. Shimada, T.; Wunsch, R. M.; Hanna, I. H.; Sutter, T. R.; Guengerich, F. P.; Gillam, E. M. J. Recombinant human cytochrome P450 1B1 expression in Escherichia coli. *Arch. Biochem. Biophys.* **1998**, *357*, 111-120.